Spectroscopic Diagnosis of a Dense Hydrogen Plasma Source

E. Alderson

August 2008

UWFDM-1345

Master's thesis.

FUSION TECHNOLOGY INSTITUTE

UNIVERSITY OF WISCONSIN

MADISON WISCONSIN

Spectroscopic Diagnosis of a Dense Hydrogen Plasma Source

E. Alderson

Fusion Technology Institute
University of Wisconsin
1500 Engineering Drive
Madison, WI 53706

http://fti.neep.wisc.edu

August 2008

UWFDM-1345

Master's thesis.

Spectroscopic Diagnosis of a Dense Hydrogen Plasma Source

by

Eric Christopher Alderson

Thesis submitted in partial fulfillment of

the requirements for the degree of

Master of Science

(Nuclear Engineering & Engineering Physics)

at the

UNIVERSITY OF WISCONSIN-MADISON

2008

Abstract

Diagnostics of high temperature and density plasmas is a challenging study that is necessary for effective utilization and development of plasma sources. There are a variety of plasmas that are not suitable to extended physical probe surveys due to probe degradation in the energetic environment. Also, RF fields and magnetic fields can add complication to interpretation of probe results that are nontrivial to overcome. However, high density plasma sources are being applied for a variety of applications, and knowing the plasma parameters is valuable for assessing the effectiveness of the plasma source utilization.

One plasma diagnostic method that is rapidly maturing is plasma emission spectroscopic analysis. By analyzing the light radiated from the plasma it may be possible to determine some plasma properties remotely. Thus the work detailed in this thesis utilizes molecular physics and collisional radiative (CR) modeling coupled with emission observations to remotely measure the properties of a hydrogen plasma in a helicon plasma source that is utilized as an ion source for the HELIOS fusion experiment at the University of Wisconsin.

This work begins by exploring the background and development of the helicon plasma source as well as the the applied state spectroscopic diagnosis. This study is then applied to the helicon source, a device that has proved impossible to study using traditional plasma probes, as the plasma was energetic enough to melt the high temperature plasma probes.

This campaign produced results that are comparable to contemporary helicon sources

in hydrogen: electron temperature on the order of 5 eV and electron density on the order of 10^{11} cm^{-3}. Gas temperature in the helicon source was also measured to be typically about 500 K. The atomic to molecular density ratio was between 10 and 27. Using the obtained electron density and temperature it is possible to compare the Bohm current limit that the helicon source theoretically can produce with the actually produced plasma current. This is essential to assess the potential for optimization of ion extraction from the helicon source. The helicon source under study has produced a maximum of 30 mA in deuterium, while the results of this work indicate that the helicon source should be able to produce a maximum of 75 mA of deuterium current.

Acknowledgments

There are a variety of people who have contributed to this work, and it is my pleasure to thank the foremost of them here.

To begin with, thanks go to David Grainger and the Grainger Foundation for the funding of this work, in support of the UW-IEC Advanced Fusion Fuels Project. I have been proud to contribute to the exceptional work underway in IEC studies at the University of Wisconsin and as a part of the larger University of Wisconsin Fusion Technology Institute.

Within the UW IEC research group my work had drawn invaluable support from all members, present and past. Special thanks go to Brian Egle, David Boris and Sam Zenobia, who have readily participated technical consultation and discussion. Also Dr. Gregory Piefer, who built the helicon source under study in this work, and was regularly available to provide his technical insight, both on the device he constructed, and his wider expertise of plasma physics. It has been thrilling to work alongside individuals of their ability and aptitude.

Thanks goes to Dr. Keiji Sawada of Shinshu University who made available, upon request, the source code for the collisional radiative model he built, which was used in this work. The model is a powerful tool that proved very valuable to this work.

Dr. Joe Khachan of the University of Sydney has been incredibly generous in providing consultation and experience in plasma physics and spectroscopy. It was his advice that helped this work find focus when it was still largely conceptual. His wide experience in technique and knowledge of the relevant technical literature has helped me to solve numerous technical problems and questions.

Dr. John Santarius has been a pillar of support in this work, providing a ready depth of theoretical grounding and experience and has always been available to consider my difficulties and lend his physical understanding. He has as been invaluable in providing enlightening and inspiring discussion, both on the topics relevant to this work and the wider field of physics.

My advisor, Dr. Gerald Kulcinski, has guided me though my graduate career adroitly, and for that he will always have my gratitude. His enthusiasm for a variety of topics is why I choose to apply to the Nuclear Engineering and Engineering Physics program at the University of Wisconsin in the first place, and I was thrilled when I was invited to join his IEC group. I continue to be excited to be a part of the quality and creative work he directs.

The non-technical support I have received also deserves special mention. A variety of friendships, near and far, have influenced my life in profound ways, and I am much obliged. My wider family too has shaped me in multitudinous ways; I have worked hard to make them all proud, from my great-grandmother to my youngest cousin. My sister has become, not only my sibling, but my longest friend over our years growing up. My mother and father have shaped me into the man I am, and I can't begin to do justice all they have done for me.

Finally, my wife's love, patience, support, and effort deserves the deepest thanks. You have shared so much with me, and made my life so much more. I am always eager to continue our adventure together! *Tu esi vislabāka, un Es Tevi mīlu, ļoti, ļoti.*

Table of Contents

Table of Figures

Table of Tables

I-A) Introduction - Motivation

The diagnosis of a steady-state, dense, laboratory plasma source has developed into an important study, as these dense plasmas are being utilized as ion sources for a variety of applications. Characterization of a dense laboratory plasma state is not trivial and remote diagnosis is ideal, as the classical probe analysis can be disruptive to the plasma, suffer degradation from particle bombardment, and introduce impurities to the plasma. With the maturity of Collisional Radiative (CR) modeling, the evaluation of a dense plasma through emission intensity spectroscopy analysis is potentially possible [I-1,2,3].

This work will examine a hydrogen plasma in a helicon source, utilized as an ion source for a fusion experiment; the purpose is to remotely diagnose the gas temperature, atomic to molecular ratio, plasma density, and electron temperature of the helicon source plasma. Determination of these properties then may be used to determine how well the device is being employed as an ion source. This method is valuable in aiding the utilization of the helicon source as an ion source for a variety of applications, from industrial plasma processing to space propulsion.

This method is applicable not only to helicon sources, but also to strongly radiating plasmas where light pollution is minimal and there exists a clear view of the plasma. The method explored in this work can be applied to a variety of RF plasmas and DC discharges, as well as helicon sources. Further, this methodology may be applicable to other species of plasma, when the governing physics is well characterized.

I-B) Spectroscopic – Collisional Radiative Plasma Diagnostic Approach

The remote diagnosis of a dense hydrogen plasma can be achieved based on emission spectroscopy. This process is outlined in Figure I-2 as a flow chart, and the specifics of these steps are detailed in the following sections. The key for standard flow chart symbols is shown in Figure I-1.

The collected spectroscopic data must be corrected to true intensity measurements, based on photon energy and quantum efficiency of the spectrometer system. Using the molecular line emission it is possible to determine the molecular gas temperature, drawing on the the molecular physics assembled by Astashkevich [I-4]. The gas temperature, with the gas pressure, allows the gas density to be estimated. The ionization fraction can be found using the gas density once the electron density is determined.

To determine the atomic to molecular ratio (H/H_2) an electron temperature must be assumed, initially based on review of the relevant literature. Using the published Lavrov results [I-3] that model atomic and molecular transition rate coefficients and the relevant measured intensity ratios, it is possible to estimate the H/H_2 ratio. The H/H_2 ratio is weakly dependent on electron temperature below 12 eV, allowing some latitude in this step of the iterative process. This H/H_2 ratio is used in the generation of theoretical intensity atomic emission intensity ratios.

The CR model is used to generate theoretical rate coefficients based on electron density and electron temperature. The estimated H/H_2 ratio and the theoretical rate

coefficients for a variety of plasma conditions are used to predict the Balmer line intensity ratios for a variety of plasma conditions. Agreement between the theoretical and measured Balmer line intensity ratios confirms that the CR model conditions and observed plasma are in accord.

Intensity ratios for multiple lines should be compared to confirm the model is correctly describing the plasma observed. If multiple measured ratios agree with the theoretical ratios on the electron temperature and density, then the plasma's preliminary diagnosis is completed. The preliminary diagnosis of the electron temperature should be compared with the initial electron temperature assumed to determine the H/H_2 ratio. If the preliminarily diagnosed electron temperature is not substantially different from the electron temperature used to predict the H/H_2 ratio (and there by producing a substantially divergent H/H_2 ratio) the diagnosis can then stand as the final diagnosis.

The plasma is not sufficiently described by the CR model used if the multiple observed ratios do not agree at any electron temperature and electron density. There are a variety of reasons why this could be, such as processes happening within the plasma that are not reflected in the model or an assumption of the model is not correct for the plasma under study.

In the case that this method of diagnostic is not viable, other options must be explored. Every diagnostic method has inherent advantages and disadvantages. A microwave interferometry diagnostic is a robust way to remotely determine the electron density from a steady state plasma source [I-5]. Use of a plasma probe is another plasma diagnostic that can be applied effectively to many plasmas, though the usage of the probe

must be tailored to the plasma under study. Other spectroscopic plasma diagnostic methods exist, but the utility of these methods must be examined individually for each plasma under

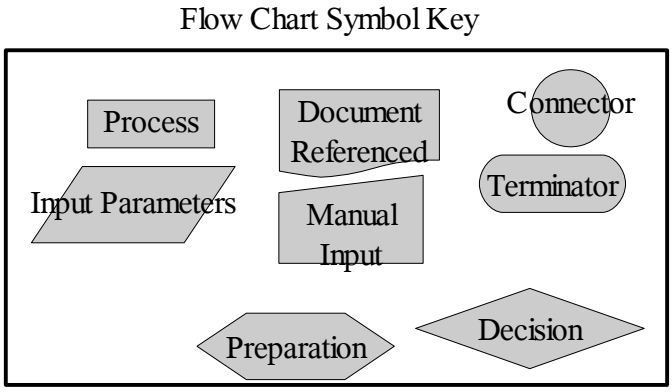

Figure I-1: Standard symbols used in flow chart in Figure I-2

study.

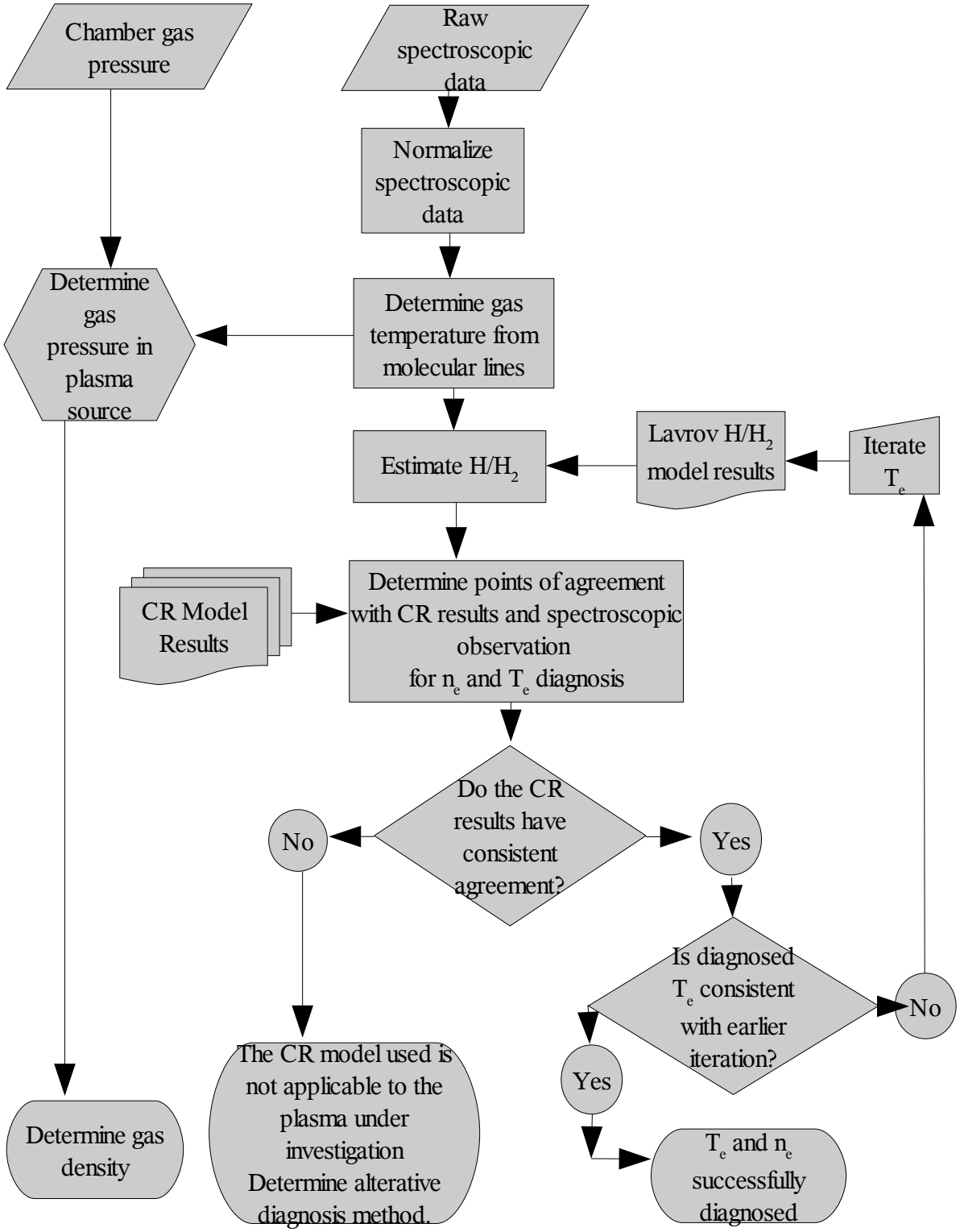

Figure I-2: Flow Chart of spectroscopic diagnosis process utilizing Collisional Radiative Modeling (CR)

References for Chapter I

I-1 D. Schieber, S. Gavril, and MS Erlicki, "Electron temperature determination in a low density helium plasma," Plasma Physics 12.11 (1970): 897-9.

I-2 K. Sawada, K. Eriguchi, and T. Fujimoto, "Hydrogen-atom spectroscopy of the ionizing plasma containing molecular hydrogen: Line intensities and ionization rate," Journal of Applied Physics 73 (1993): 8122.

I-3 B. P. Lavrov, A. V. Pipa, and J. Ropcke, "On determination of the degree of dissociation of hydrogen in non-equilibrium plasmas by means of emission spectroscopy: I. The collision-radiative model and numerical experiments," Plasma Sources Science & Technology 15.1 (2006): 135-46.

I-4 SA Astashkevich, et al, "Radiative characteristics of 3p Sigma, Pi; 3d Pi-, Delta-states of H2 and determination of gas temperature of low pressure hydrogen containing plasmas," Journal of Quantitative Spectroscopy and Radiative Transfer 56.5 (1996): 725-51.

I-5 DJ Kraft, et al, "Analysis of multifrequency interferometry in a cylindrical plasma," Review of Scientific Instruments 77 (2006): 10E910.

II-A) Historical Overview of Previous Work – Introduction

This work reviews the methodology to remotely characterize a dense hydrogen plasma through spectroscopic analysis and is primarily dependent on the development in the fields of optical diagnosis and the helicon source plasma source used in this work. A general discussion of some of the literature on these topics will be presented, motivated with brief treatment of the progress in these fields. The theoretical foundation for this work will be addressed in the following chapters with specificity to the application studied.

II-B) Optical Diagnostics

The first observations of plasmas were made possible by the light radiated from plasma . It was not until the advent of modern physics and the understanding of the shell model and allowed transitions that it was possible to make sense of the mechanism whereby electromagnetic radiation is emitted from an excited atom or molecule when it de-excites.

Armed with this understanding, physicists have tried to diagnose the plasma conditions based on the light emitted from the plasma; this study is broadly called “plasma spectroscopy”. Such diagnostics methods are of interest to laboratory plasma physics experiments as well as astrophysics; however, the vast range of plasma temperatures and densities that plasma spectroscopy may be applied to has thus far precluded a unified, diagnostics methodology [II-1].

Optical diagnostics have the advantage of being remote and non-perturbing. Physical

probes must be inserted into a plasma for use, can only diagnose the plasma locally, and may perturb the plasma and as a result disrupt the local readings. Further, Radio Frequency (RF) waves can disrupt probe readings, unless the probe is frequency compensated [II-221]. Also, probes can be eroded by sputtering that can both generate metallic impurities (which is detrimental to plasma assisted film deposition applications) and degrade the probe geometry, reducing the reading uniformity with time, and thus require periodic maintenance.

Meanwhile, an optical diagnostic does not perturb or contaminate the plasma. The reading yields a field-of-view averaged plasma measurement for optically thin plasmas. The optical reading is not affected by magnetic field or RF field and with a fast enough detector, optical measurements can be used to diagnose the plasma response on the RF cycle time scale [II-3]. Further, once the optical system is properly set up it requires little maintenance and, as the observation is remote, the measurement apparatus is not degraded.

Some of the earliest work in spectroscopic plasma diagnosis was done through line broadening analysis [II-4]. The radiation from an electron transition would be sharp within the limits of the uncertainty principle, thereby producing a Lorentz profile, except for physical interactions that broaden the radiation distribution. The broadening mechanisms are Doppler broadening and pressure broadening, which is given a fuller treatment in Appendix-A.

This work has progressed for many decades, but the method requires sophisticated spectroscopy and a foreknowledge of the mechanisms occurring in the plasma under study. Further, it is impossible to accurately diagnose the effects of temperature broadening on a spectral line profile (through Doppler shift) without knowing in advance the pressure

broadening effect (through various phenomena), or vice versa. Due to this difficulty, it has been judged that line width diagnostics are probably not appropriate for a modest laboratory plasma diagnostic.

The advent of collisional radiative (CR) modeling opens up a new avenue of spectroscopic diagnostic of plasmas, particularly for laboratory plasmas [II-5,6,7]. A collisional radiative model assumes some plasma parameters such as electron energy distribution, electron temperature, and gas temperature. Then, using excitation cross sections and excited states mean lifetimes assembled by atomic physicists, the relative emission line intensities can be predicted as dependent on plasma parameters. The results of this model are compared with observation for agreement to perform the diagnosis.

This sort of analysis has been done on various plasma sources. The concept was first proposed in 1955 [II-8], but preliminary results were not published until 1962 [II-9]. The historical scarcity of relevant atomic physics data has constrained the development of this technique. However, limited theoretical development was carried out through the 60's and into the 70's and the technique was limited to plasmas with well defined atomic mechanisms and interactions. Development accelerated in the mid 80's in as a result of the advancement of atomic interactions physics, with significant work done on CR modeling in Eastern Europe and Japan [II-1, 10]. The examination of tokamak edge plasma physics significantly motivated CR modeling development in hydrogen. It was not until the late 90's that the CR modeling diagnostic method had matured to the point to applicability across a wide variety of plasmas. Microwave discharge plasmas have been diagnosed via this method only recently[II-11,12]. The validity of CR modeling as a diagnostic tool in a helicon source light

ion plasma was established as recently as 2001 [II-13].

Diagnosing a plasma's gas temperature is necessary but challenging. It is not uncommon to assume a room temperature gas though verification is valuable. The gas rotational temperature can also be diagnosed spectroscopically, through molecular line intensities coupled with relevant excitation equations [II-14]. In a reasonably collisional plasma, one can safely assume the rotational and vibrational gas temperature are equilibrated at roughly the kinetic gas temperature [II-15]. This temperature, coupled with an estimate of pressure yields a neutral particle density.

II-C) The Helicon Source

The helicon source is a plasma source known for its high ionization efficiency, regularly able to produce 10^{19}-10^{20} ions/m^3 with RF power on the order of hundreds of watts, and magnetic fields under 0.1 Tesla in nitrogen or argon [II-16]. This efficiently produced ion density can have a variety of applications.

The existence of low-frequency electromagnetic waves in laboratory plasmas was discovered as early as the 1960's [II-17], though it was not until the 1980's that the helicon plasma source was widely recognized as a highly efficient gaseous plasma ion source[II-18]. While the helicon source has demonstrated a remarkable performance, the device is not particularly well understood.

It is known that the helicon wave dispersion relation is that of a cylindrically bounded whistler wave. The dispersion relation of this wave is well known, however the helicon source exhibits several phenomena that are not understood and the theory remains rather

controversial. A variety of parameters can have impact on plasma density, though the mechanisms at work are not always known. A helical antenna produces a higher density plasma than a more cylindrical Nagoya antenna, and while the antenna modifies the wave mode, there is no theory that can explain the helicon source plasma density's mode dependence [II-19]. The direction of rotation as the helicon wave propagates (the handedness of the wave) can substantially impact the plasma density as well [II-20]. Despite extensive exploration of the helicon device[II-21], helicon source theory has not matured to the point of having accurate predictive capability, and development of the helicon source has been largely empirical [II-22].

As helicon source development has been largely empirical, it is important to have accurate diagnostics of the plasma inside the helicon source. However, diagnosis is difficult due to the high particle density and energy, as well as RF and B fields complicating probe usage. Physical probes may not survive the harsh environment in high power helicon source operating regime and in situations where the probe can survive the helicon source plasma environment, an RF compensated Langmuir probe is required for accurate readings[II-2]. Also, physical probes can locally disrupt the plasma, producing measurement uncertainty, so a noninvasive diagnostic is preferable. It is possible to diagnose an ion beam extracted from a helicon source with physical probes, but that may not be a true representation of the state of the helicon source plasma, as beam extraction efficiency is highly dependent on a variety of variables besides plasma density.

Regardless, the helicon source has a variety of applications and further potential applications are under exploration. An ion beam can be extracted from the high density

plasma to produce an ion beam for fusion applications. This has been done in an Inertial Electrostatic Confinement device [II-23] as well as beam target sources [II-19].

The use of the helicon source plasma as an ion source for plasma processing has been explored and validated for use in semiconductor manufacturing [II-24,25]. This application has not become standard in industry due to complications in practice. While it is possible to compensate for these complications, the helicon source has not evidenced an obvious advantage over conventional plasma processing techniques meriting the broad application of helicon sources in plasma processing. However, the plasma processing field is still developing and is constantly innovating, so the high efficiency production of ions may be very useful to the plasma processing field in the future.

Another use of the helicon source being researched is electric propulsion for spacecraft [II-26]. The VASIMR (Variable Specific Impulse Magnetoplasma Rocket) thruster utilizes the helicon source as an efficient high density ion source; extracted ions are then heated and magnetically directed to provide thrust. The variable specific impulse nature of the thruster allows for a selectable trade-off between thrust and efficiency, which is attractive for high efficiency-low thrust space propulsion on high energy missions.

References for Chapter II

II-1 H.R. Griem, Principles of Plasma Spectroscopy (Cambridge: ; New York :; Cambridge University Press, 1997) 366.

II-2 S.N. Ghosh, et al, "Study of High-Density Helicon-Plasma Generation and Measurement of the Plasma Parameters by Using a Frequency-Compensated Langmuir Probe," Journal of the Korean Physical Society 48.5 (2006): 908-13.

II-3 T. Gans, V. Schulz-von der Gathen, and HF Dobele, "Time dependence of rotational state populations of excited hydrogen molecules in an RF excited plasma reactor," Plasma Sources Science and Technology 10.1 (2001): 17-23.

II-4 H.R. Griem, Spectral Line Broadening by Plasmas (New York: Academic Press, 1974) 408.

II-5 K. Sawada, K. Eriguchi, and T. Fujimoto, "Hydrogen-atom spectroscopy of the ionizing plasma containing molecular hydrogen: Line intensities and ionization rate," Journal of Applied Physics 73 (1993): 8122.

II-6 K. Sawada and T. Fujimoto, "Effective ionization and dissociation rate coefficients of molecular hydrogen in plasma," Journal of Applied Physics 78 (1995): 2913.

II-7 B. P. Lavrov, A. V. Pipa, and J. Ropcke, "On determination of the degree of dissociation of hydrogen in non-equilibrium plasmas by means of emission spectroscopy: I. The collision-radiative model and numerical experiments," Plasma Sources Science & Technology 15.1 (2006): 135-46.

II-8 D. Schieber, S. Gavril, and MS Erlicki, "Electron temperature determination in a low density helium plasma," Plasma Physics 12.11 (1970): 897-9.

II-9 C.C. Lin and R. M. S. John, "Collisional Excitation Transfer to the 4 1D State in Helium by Multiple State Mechanism," Phys Rev 128 (1962): 1749.

II-10 B.P. Lavrov, VN Ostrovsky, and VI Ustimov, "Non-Franck-Condon transitions in the electron impact excitation of molecules 11. Semi-empirical approach: transitions in H2," J.Phys.B: At.Mol.Phys 14 (1981): 4701-18.

II-11 K. Behringer, "Diagnostics and modelling of ECRH microwave discharges." Plasma Physics and Controlled Fusion 33.9 (1991): 997-1028.

II-12 B.P. Lavrov, et al, "uv continuum emission and diagnostics of hydrogen-containing nonequilibrium plasmas," Physical Review E 59.3 (1999): 3526-43.

II-13 R.F. Boivin, JL Kline, and EE Scime, "Electron temperature measurement by a helium line intensity ratio method in helicon plasmas," Physics of Plasmas 8 (2001): 5303.

II-14 S.A. Astashkevich, et al, "Radiative characteristics of 3p Sigma, Pi; 3d Pi-, Delta-states of H2 and determination of gas temperature of low pressure hydrogen containing plasmas," Journal of Quantitative Spectroscopy and Radiative Transfer 56.5 (1996): 725-51.

II-15 M. Shimada, G. R. Tynan, and R. Cattolica, "Rotational and translational temperature equilibrium in an inductively coupled plasma," Journal of Vacuum Science & Technology A: Vacuum, Surfaces, and Films 24 (2006): 1878.

II-16 IS Hong, "Ion-beam characteristics of novel helicon ion sources for different plasma parameters," Review of Scientific Instruments 71.3 (2000): 1385.

II-17 C. M. Franck, Experiments on Whistler Wave Dispersion in Bounded Magnetised Plasmas s. n, 2003).

II-18 R.W. Boswell and FF Chen, "Helicons-the early years," Plasma Science, IEEE Transactions on 25.6 (1997): 1229-44.

II-19 H.D. Jung, et al, “Development of a compact Helicon ion source for a neutron generator” ICOPS 2003.IEEE Conference Record-Abstracts. The 30th International Conference on Plasma Science (2003).

II-20 F.F. Chen and RW Boswell, "Helicons-the past decade," Plasma Science, IEEE Transactions on 25.6 (1997): 1245-57.

II-21 Gilland. J H, , PhD (Nuclear Engineering and Engineering Physics), University of Wisconsin - Madison, 2004.

II-22 MD Carter, et al, "Comparing experiments with modeling for light ion helicon plasma sources," Physics of Plasmas 9 (2002): 5097.

II-23 G.R. Piefer, Performance of a Low-Pressure, Helicon Driven IEC 3He Fusion Device, UW-Dissertation, (December 2006).

II-24 F.F. Chen, J.D. Evans, and G.R. Tynan, "Design and performance of distributed helicon sources," Plasma

References for Chapter II

Sources Science and Technology 10.2 (2001): 236-49.

II-25 JTC Lee, et al, "Comparison of advanced plasma sources for etching applications. V. Polysilicon etching rate, uniformity, profile control, and bulk plasma properties in a helical resonator plasma source," Journal of Vacuum Science & Technology B: Microelectronics and Nanometer Structures 14 (1996): 2510.

II-26 T.W. Glover, et al, Principal VASIMR Results and Present Objectives: AIP Conf. Proc 749, 1 (2005): 976-82.

III-A) Overview of Gas Temperature and Density Measurement - Introduction

An optical measurement of gas temperature in a plasma is valuable as a noninvasive and non-perturbing method for diagnosing the gas properties of a plasma, in this case considering a hydrogen plasma. The gas temperature is determined from the emission profile of molecular lines. With knowledge of the gas temperature, and with a determination of gas pressure, it is possible to determine the gas density. Knowledge of the gas properties will lay the foundation for the full diagnosis of the plasma characteristics.

III-B) Determination of Gas Temperature through Molecular Lines

The first step in diagnosing a helicon source plasma is determining the gas temperature. The gas is heated by the energetic charged particles within the plasma via collisions, and cooled primarily by radiation. The gas temperature can, along with gas pressure, yield gas density.

Gas temperature cannot be measured directly in a helicon source at high density operation, and no remote method to directly measure gas temperature in a helicon source is known to exist. However, two indirect methods of measuring the gas temperature within the helicon source may be utilized.

The simplest indirect measurement of the gas temperature inside the helicon source is to measure the wall temperature of the quartz tube that contains the helicon source plasma.

This tube reaches an equilibrium between the hot gas heating the tube walls, and radiation and convection that removes energy. The magnetic field prevents the bulk of the charged particles from impacting the quartz tube, but the efficiency this mode of energy transfer is not known. It is only known that the gas temperature must be higher than the measured wall temperature.

It is also possible to determine the rotational temperature spectroscopically from molecular line emission [III-1]. In a collisional plasma the vibrational, rotational, and kinetic (gas) temperature are roughly equilibrated via collisions [III-2]. The relevant plasmas are not necessarily sufficiently collisional, but comparisons can be made with the quartz wall temperature to determine if the measured rotational temperature is approximately the minimum temperature for an order of magnitude measurement. Once an estimate of the electron temperature is made, the Debye length and gas mean free path can be estimated to assess collisionality.

Not only do electrons have specified orbital states, but they also have allowed rotational and vibrational molecular states; the allowed orbital, rotational and vibrational states of the electron are called rovibronic states. Rovibronic molecular states, like electron orbital states, have known allowed states and transitions, as defined by the quantum mechanics of the molecular system. For each electron there exists a series of allowed rotational and vibrational states of the molecule. An example for the first few states and transitions in hydrogen is diagrammatically illustrated in Figure III-1 [III-3].

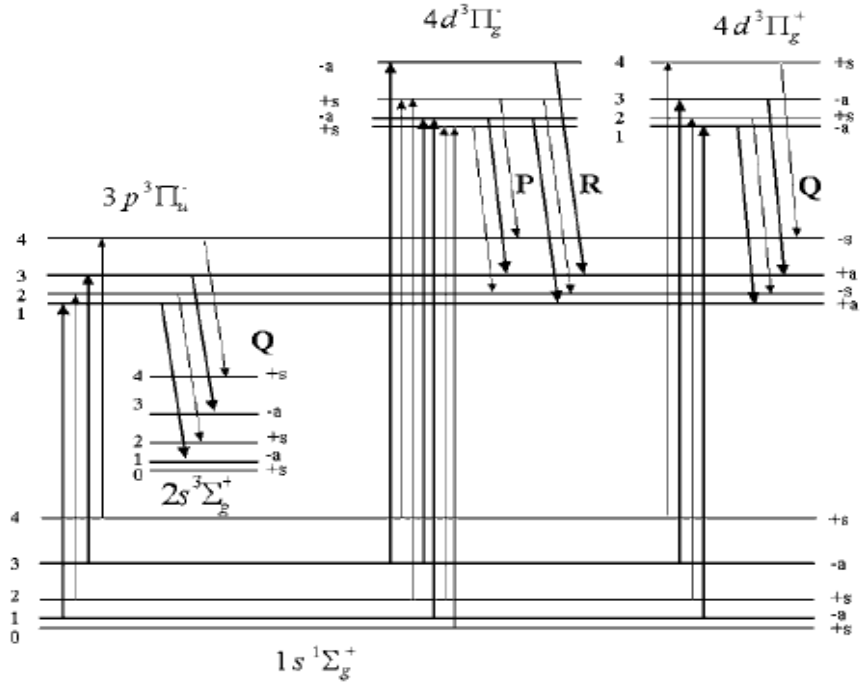

Figure III-1: Term diagram of Hydrogen illustrating a Q branch of the Fulcher-α band, and the P-, Q-, and R- branches from the Π states of the 4d level into the upper Fulcher-α levels. Upward arrows represent electronic excitation, and downward represent transitions that emit a photon [III-3].

The transitions for the electrons in the molecular system are described as $(n',v',N')\rightarrow(n'',v'',N'')$; where n is the primary quantum number, v is the vibrational quantum number, and N is the rotational quantum number of the molecule describing the electron state. De-excitation occurs via spontaneous emission, and emits a characteristic wavelength of light.

A spontaneous transition produces electromagnetic radiation with an intensity described by

$$I_{n'',v'',N''}^{n',v',N'} \propto N_{n',v',N'} A_{n'',v'',N''}^{n',v',N'} h\nu \qquad \text{(III-1)}$$

where $I_{n'',v'',N''}^{n',v',N'}$ is the line intensity, in photons per unit volume per second, from the original state to the final state (this is proportional to transitions per unit volume per second), $N_{n',v',N'}$ is the population of molecules in the (n',v',N') state, $A_{n'',v'',N''}^{n',v',N'}$ is the transition probability for spontaneous emission, also called the Einstein Coefficient for spontaneous emission, and hν is photon energy where h is Planck's constant and ν is the photon frequency. The parameter $A_{n'',v'',N''}^{n',v',N'}$ has units of s^{-1}, and the inverse of this value is the mean lifetime of the excited molecular state. The value of $A_{n'',v'',N''}^{n',v',N'}$ used is an empirically measured quantity when possible as agreement with theoretical calculations has been low.

If the rotational levels for the (n',v') state follow a Boltzmann distribution, $N_{n',v',N'}$ is described by

$$N_{n',v',N'} \propto c_{n',v'} g_{a,s} (2N'+1) \exp\left(\frac{-hcE_{n',v',N'}}{kT_{rotational}(n',v')}\right) \qquad \text{(III-2)}$$

where, $c_{n',v'}$ is a normalization constant $g_{a,s}$ is the degeneracy of the emission line, caused by nuclear spin, $E_{n',v',N'}$ is the energy of the rovibrational level (commonly measured in cm^{-1} in atomic physics), h is Plank's constant, c is the speed of light, and k is Boltzmann's constant [III-1]. Therefore, we find with sufficient knowledge of the relevant

molecular physics constants and a measure of intensity of molecular lines, it is theoretically straightforward to determine rotational temperature.

The relevant constants for the hydrogen molecule have been assembled by Astashkevich [III-1]. There are a variety of bands closely spaced, in some cases overlapping. This requires some selectivity in choice of molecular lines. The choice of lines used is discussed in Chapter VII-B.

The relatively low intensity of the H_2 molecular lines complicates the analysis. Molecular lines can be found well away from the intense atomic Lyman transitions, but it can be difficult to resolve the weak molecular lines from the background noise, particularly in an apparatus utilizing an uncooled detector. Two strategies exist to improve the quality of the measurements.

First, rather than observing a pure hydrogen plasma, a small impurity of a diatomic gas with more intense atomic lines can be added to the flow into the plasma. Once a suitable impurity that exhibits strong molecular lines with well characterized molecular physics is found, the impurity is added to the flow until the molecular lines are distinguishable. So long as the impurity remains a small constituent of the plasma it can be assumed that the bulk of the plasma sets the gas temperature. However, if the impurity becomes too large a constituent of the plasma, the plasma properties are not dominated by the hydrogen, and the measured temperature no longer reflects that of a true hydrogen plasma.

Nitrogen is a good candidate impurity for this purpose[III-4]. The N_2 lines are more intense than the H_2 lines, and the molecular transitions are well diagnosed. A roughly 5% impurity has been used successfully to accurately diagnose a hydrogen plasma's gas

temperature.

Secondly, it is possible to examine transitions that have a common electronic and vibrational quantum number (n',v'), but different rotational quantum numbers (N'). These transitions have the normalization constant $c_{n',v'}$ in common. This allows comparisons if Equations (III-1) and (III-2) are combined:

$$I^{n',v',N'}_{n'',v'',N''} \propto A^{n',v',N'}_{n'',v'',N''} c_{n',v'} g_{a,s}(2N'+1)\exp\left(\frac{-hcE_{n',v',N'}}{kT_{rotational}(n',v')}\right) \quad \text{(III-3)}$$

Equation (III-3) can be rearranged:

$$\frac{I^{n',v',N'}_{n'',v'',N''}}{A^{n',v',N'}_{n'',v'',N''} g_{a,s}(2N'+1)} \propto c_{n',v'}\exp\left(\frac{-hcE_{n',v',N'}}{kT_{rotational}(n',v')}\right) \quad \text{(III-4)}$$

Then, the natural log can be taken of both sides:

$$\ln\left(\frac{I^{n',v',N'}_{n'',v'',N''}}{A^{n',v',N'}_{n'',v'',N''} g_{a,s}(2N'+1)}\right) = \ln(C_{onst}) - \frac{hcE_{n',v',N'}}{kT_{rotational}(n',v')} \quad \text{(III-5)}$$

So, that if transitions with common (n',v') are measured and $\ln\left(\frac{I^{n',v',N'}_{n'',v'',N''}}{A^{n',v',N'}_{n'',v'',N''} g_{a,s}(2N'+1)}\right)$ is plotted against $\frac{hcE_{n',v',N'}}{k}$, the slope of the line is $\frac{-1}{T_{rotational}(n',v')}$.

This has the combined advantage of making proportionality constants immaterial to the determination of temperature and reducing the propagated error from measurements in

each line due to averaging in determining the average slope.

III-C) Determining Gas Density

Once the gas temperature has been determined it is possible to determine the gas density. This is straightforward from the ideal gas law:

$$P = nkT \qquad \text{(III-6)}$$

once the pressure in the helicon source is known.

There are various ways to determine the gas pressure inside the helicon source, though direct measurement is typically non-trivial. A helicon source plasma is necessarily contained in a cylindrical chamber, surrounded by magnets and an antenna. The cylindrical chamber must withstand extreme conditions while maintaining a low pressure. Thus making it difficult to accommodate a probe for pressure measurement.

A helicon source has a gas flow in and out of the device. Using gas flow conduction theory, flow rate or pumping speed, and an accurate pressure reading up or down stream of the helicon source allows for a determination of gas pressure in the helicon source.

Conduction behavior is dependent on the flow regime, parameterized by $k = \frac{\lambda}{d}$, where λ is the collisional mean free path (m.f.p.) and d is the gas volume diameter. Where $k \ll 1$ the gas flow is considered viscous, where $k > 1$ the flow is molecular, and where $0.01 < k < 1$ the flow is in transition or in a Knudsen (gas-kinectic) state [II-5].

In the application explored for this work, the flow is in the Knudsen state. Also, at the outlet aperture, the pressure outside the helicon source is significantly lower than on the helicon source side. This is described as choked flow.

In choked flow the conductance through an aperture is described by

$$C_{aperture} = 0.85 A \left(\frac{kT}{m} \frac{2\gamma}{\gamma+1} \right) \left(\frac{2}{\gamma+1} \right)^{\frac{\gamma}{\gamma+1}} \quad \text{(III-7)}$$

where A is aperture area in m^2 and γ is the specific heat ratio, which is 7/5 for diatomic gases [II-5].

With the calculated conductance through the aperture and known pumping speed of the vacuum pump for the relevant gas the ratio may be set up:

$$C_{aperture} P_{helicon} = S_{pump} P_{sink} \quad \text{(III-8)}$$

where S_{pump} is the pumping speed of the relevant gas in the 'sink' chamber vacuum pump, P_{sink} is the measured pressure in the chamber that the helicon source vents to, and $C_{apature}$ is the calculated aperture conductance.

Then $P_{helicon}$ is given by

$$P_{helicon} = \frac{S_{pump} P_{sink}}{C_{aperture}} \quad \text{(III-9)}$$

Then the gas density in the helicon source is described by:

$$n_{gas} = \frac{P_{helicon}}{kT_{gas}} \quad \text{(III-10)}$$

References for Chapter III

III-1 SA Astashkevich, et al, "Radiative characteristics of 3p Sigma, Pi; 3d Pi-, Delta-states of H2 and determination of gas temperature of low pressure hydrogen containing plasmas," Journal of Quantitative Spectroscopy and Radiative Transfer 56.5 (1996): 725-51.

III-2 M. Shimada, G. R. Tynan, and R. Cattolica, "Rotational and translational temperature equilibrium in an inductively coupled plasma," Journal of Vacuum Science & Technology A: Vacuum, Surfaces, and Films 24 (2006): 1878.

III-3 T. Gans, Schulz-von der Gathen, V., and HF Dobele, "Time dependence of rotational state populations of excited hydrogen molecules in an RF excited plasma reactor," Plasma Sources Science and Technology 10.1 (2001): 17-23.

III-4 U. Fantz and B. Heger, "Spectroscopic diagnostics of the vibrational population in the ground state of H 2 and D 2 molecules," Plasma Phys Control Fusion 40 (1998): 2023-32.

III-5 J.F. O'Hanlon, A User's Guide to Vacuum Technology, 3rd ed. (New York: John Wiley and Sons Inc., 2003).

IV-A) Overview of Collisional Radiative Modeling Theory - Introduction

This section will detail Collisional Radiative (CR) modeling and its use in this thesis. To begin with, the theory of CR modeling will be considered, detailing the state of the theory and describing its development. Once the fundamentals of CR modeling are outlined, the process of determining atomic to molecular species ratio will be explored. Following this diagnosis the electron temperature and density will be estimated.

Considering chapters III and IV in totality, we find it is in principle possible to remotely diagnose a dense hydrogen plasma's gas temperature, gas pressure, density, atomic to molecular species ratio, electron density and electron temperature in a plasma source, such as a helicon source. These approaches can be applied to other plasma sources, as well as other plasma species (i.e. He, N_2, Ar,...).

IV-B) Collisional Radiative Modeling

Collisional radiative (CR) modeling at its simplest, predicts the interactions of an electron population striking a population of atoms and molecules. Some of these interactions result in electromagnetic radiation, which can be correlated with observations to diagnose the actual plasma parameters. To apply this diagnostic method requires understanding of the interactions occurring to produce excited states, and knowing the atomic physics constants associated with these interactions.

CR modeling grew out of refinement of the simple steady state coronal (SSC) model.

The simplest SSC model assumes excitation due to a single process, described by:

$$I_{ji} = N_1 n_e \langle Q_{ji}(v_e) v_e \rangle h \nu_{ji} \quad \text{(IV-1)}$$

where I_{ji} is the radiated line intensity of the level j to the level i transition, N_1 and n_e are the atom or molecular and electron population number densities respectively, Q_{ji} is the relevant excitation cross-section, v_e is the electron velocity, h is Planck's constant, and ν_{ji} is the frequency associated with the transition [IV-1]. The value of this intensity is dependent on both density and the electron temperature distribution. A computer, using relevant databases, can predict the intensity of lines for a series of parameters.

The emission is then physically measured as photon count rate by a detector:

$$I_p(\lambda_{ji}) = N_j A_{ji} T(\lambda_{ji}) G_{syst} \quad \text{(IV-2)}$$

where I_p is the photon count rate, N_j is the population of the emitting level (the j^{th} level), A_{ji} is the Einstein spontaneous emission coefficient for the j to i transition, $T(\lambda_{ji})$ is the coefficient of transmission for the pertinent wavelength which is dependent on device response and the detector quantum efficiency, and G_{syst} is the system's geometric factor which accounts for the observed plasma volume and solid angle subtended by the collection optics. Ratios of these observations are taken to eliminate the G_{syst} term and the wavelength dependent $T(\lambda_{ji})$ factor is corrected for so the relevant measured intensities are on the same scale using known quantum efficiency or measurement of a standardized lamp.

The SSC model was further refined, to include the branching ratio, as an excited state has multiple allowed decay paths. The relevant intensity ratios are described by:

$$\frac{I(\lambda_{ji})}{I(\lambda_{kl})}=\frac{N_j h\nu_{ji} A_{ji}}{N_k h\nu_{kl} A_{kl}}=\frac{\langle\sigma\nu\rangle_{oj} h\nu_{ji} A_{ji}(\Sigma_{i<j} A_{ji})^{-1}}{\langle\sigma\nu\rangle_{ok} h\nu_{kl} A_{kl}(\Sigma_{l<k} A_{kl})^{-1}} \qquad \text{(IV-3)}$$

where $I(\lambda_{yx})$ is the intensity for the y to x transition, $(\Sigma_{x<y} A_{yx})$ is the total transition probability from level y to all levels lower than y, and $A_{yx}(\Sigma_{x<y} A_{yx})^{-1}$ is the branching ratio or ratio of the probability for a specific transition over the probability to all lower states; again, h is Planck's constant and ν_{yx} is the frequency associated with the relevant wavelength. From equation (IV-3) the wavelength dependent system calibration is taken into account when the measurement of $\frac{I_p(\lambda_{ij})}{I_p(\lambda_{kl})}$ is made. When applicable, Equation (IV-3) allows for the electron energy to be found from an intensity ratio.

The above model assumes that all observed transitions occur from excited states that are excited directly from the ground state, and all other occurrences of the relevant excited states are negligible. This model has applicability and good agreement with diagnosed plasmas for conditions where the ground state dominates the populations, however density limits do exist for this model. At higher densities other processes begin to noticeably perturb the excited population densities, these processes include volume recombination, ground state and excited atom collisions, cascading redistribution, excitation transfer collisions, and excitation from metastable states [IV-2]. Depending on the plasma, any of these processes can impact the populations present in the plasma, and an analysis must be made of when the SSC model is reasonably applicable. When it is determined that the SSC model fails, a more sophisticated model must be used; the term for this class of models is a collisional radiative

(CR) model.

The CR model typically assumes a steady state system, in which the the population of a bound level N_i is described by the expression:

$$\frac{dN_i}{dt} = n_e \Sigma_{j \neq i} S_{ji} N_j + \Sigma_{j>i} A_{ji} N_j - n_e \Sigma_{j \neq i} S_{ij} N_i - \Sigma_{j<i} A_{ij} N_i - n_e I_i N_i = 0 \qquad \text{(IV-4)}$$

where the expression $n_e \Sigma_{j \neq i} S_{ji} N_j$ describes the excitation or de-excitation of all levels j that end up in level i; $\Sigma_{j>i} A_{ji} N_j$ describes the spontaneous de-excitation from higher levels j to level i; $n_e \Sigma_{j \neq i} S_{ij} N_i$ describes excitation or de-excitation of level i from electron impact; $\Sigma_{j<i} A_{ij} N_i$ describes the spontaneous de-excitation from level i to all lower levels j; and $n_e I_i N_i$ describes the ionization rate from level i.

Each of these terms can have multiple processes associated with it. The dominant terms of this equation must be characterized for all the levels under consideration. Theoretically, an infinite number of bound levels is possible, however once the dominating lower levels have been accounted for all remaining levels are spaced close together just below the ionization energy and can be collapsed into one bound level just below the ionized state. The equations describing each level are highly coupled as well.

The applicability of this method has been verified for a variety of plasmas and plasma conditions. This includes magnetically confined fusion edge plasmas [IV-3], RF plasmas [IV-4], DC glow discharges[IV-5], inductively coupled plasmas , hollow cathode[IV-6], and helicon sources[IV-7]. At the earliest, it was used to diagnose low density helium plasmas, but it is frequently applied to argon plasmas, and has been applied to mercury plasma in a

limited fashion. The application to hydrogen plasmas has until recently been limited.

The limitations in application of the CR modeling diagnostic depend on the plasma parameters. Firstly, the intensity of the electromagnetic radiation must be detectable above background noise levels. If the plasma does not emit enough light to be measured spectroscopic measurements are useless. In an environment with a significant light pollution the signal from the plasma can be overwhelmed as well.

Secondly, there must be confidence in what dominating interactions are occurring. The simple assumptions may become invalid in some regimes as low level interactions perturb the emission intensities. It is therefore required that the CR model used should be validated experimentally or theoretically for the existing regime of the diagnosed plasma. Many of the relevant interaction cross-sections and Einstein coefficients are not known, particularly for the very short half-life reactions. Theoretical calculations can be used to fill in the gaps in the experimental database, but theory and empirical values presently differ in some cases by more than an order of magnitude. Further, a high confidence in the cross-section databases is necessary, which is a consideration that has greatly limited the application of this diagnostic tool until recently, as disagreement in databases plagued atomic physics for many years. Recent crossed-beam experiments have improved confidence in some of these cross-section databases substantially.

Thirdly, the plasma must be in a regime where the radiation is sensitive to the plasma parameters, as some transitions can become insensitive to electron temperature and density and have little diagnostic value as a result. This is particularly challenging in plasmas with a high electron temperature. Intensity ratios for some plasmas lose diagnostic capability or

precision at high temperature. Further, some intensity ratios become insensitive to electron temperature at lower temperatures. Also, some emissions become very dependent on the plasma parameters, making the possible error bars large. All of this reinforces the need for experimental or theoretical validation of the diagnostic for the operation regime.

Finally, there must be a reasonably high confidence in the electron population distribution. Most CR models are based on a Maxwellian energy distribution assumption. If the electron population has an atypical population distribution, the CR model must reflect that for the model to correctly predict the plasma transition coefficients. For many years there was doubt regarding the applicability of CR models to the helicon source plasma. It was hypothesized that the helicon source was an especially efficient plasma source due to the generation of an electron energy distribution that was weighted more toward high energies due to hypothesized Landau damping, producing a non-Maxwellian electron energy distribution. However, a strong agreement in the low pressure regime between a SSC model diagnostic (that assumed a Maxwellian electron temperature distribution) and probe measurements both confirmed that line emission diagnostics can be a valuable helicon source plasma diagnostics and repudiated the hypothesis of a significant non-Maxwellian electron energy distribution[IV-2]. Attempts to unambiguously detect this high electron energy distribution have failed, further supporting the use of the Maxwellian electron energy distribution assumption as applied to the helicon source.

To validate the use of a CR modeling diagnostic one must identify the regimes where the model is useful. In some regimes the characteristics of the plasma interactions are not properly reflected by the generated CR model, due to poor atomic physics data or

interactions not accounted for. These regimes are in general identified through comparison of CR model results with well characterized plasmas. When possible, these plasmas are initially characterized through probe diagnostics, such as Langmuir probes. Once the applicable regimes are identified, bounds can be set on the diagnostic operations. Within the valid regimes the model may be confidently applied as a plasma diagnostic.

Two CR models are used in this work. The first is the hydrogen plasma CR model developed by Lavrov, published in 2005, which will be useful for determination of atomic to molecular Hydrogen ratio [IV-8]. This model publishes rate coefficients relating three transitions. The first two rate coefficients examined are the first two Balmer emissions, H_α (n=3 $\rightarrow$ 2) and H_β (n=4 $\rightarrow$ 2). These are measured at 656.3 nm and 486.1 nm respectively. The other rate coefficient is the molecular transition $(X^1\Sigma_g^+, v=0, N=1) \rightarrow (d^3\Pi_u^-, v=2, N=1)$. The latter state is only allowed from the former, significantly simplifying the modeling of this transition. This molecular transition is the Fulcher-α (2-2) Q1 line, which is abbreviated as the Q1 line, measured at 622.5 nm. These ratios are principally dependent on two plasma parameters, the electron temperature and the atomic to molecular ratios.

The second CR model was developed by Sawada and Fujimoto, developed primarily for diagnosis of fusion edge plasmas [IV-9,10,11,12]. The Fortran code for this model was made available by Sawada, and utilized in this work to produce a series of theoretical Balmer emission intensity ratios based on electron density and temperature, and the atomic to molecular densities predicted by Lavrov's work.

IV-C) Diagnosis of Atomic to Molecular Ratio

In a hydrogen plasma the electron temperature and the atomic to molecular ratio are the crucial plasma parameters. Diagnosis of both can be challenging in a helicon source plasma as helicon source plasmas are inhospitable to probes. Diagnosis of the electron temperature and atomic to molecular ratio using CR modeling of a hydrogen plasma is in fact coupled.

In principle, it is straightforward to diagnose the electron population as well as the atomic to molecular ratio using collisional radiative (CR) modeling coupled with spectroscopic plasma measurements. Considering the hydrogen plasma CR model diagnosis specifically, given two independent intensity ratios (requiring three intensity measurements), diagnosis is a matter of finding agreement for the intensity ratios, electron temperature and atomic to molecular ratio plasma parameter values. The intensity ratios are measured, leaving two parameters to be varied until agreement between the model and observation is reached.

The $I_{H\alpha}$ and $I_{H\beta}$ transition ratio is described by:

$$\frac{I_{3\to 2}}{I_{4\to 2}} = \frac{\left(\frac{N_H}{N_{H2}}\right) K_{dir}^{em}(T_e^{eff} \mid H_\alpha) + K_{dis}^{em}(T_e^{eff} \mid H_\alpha)}{\left(\frac{N_H}{N_{H2}}\right) K_{dir}^{em}(T_e^{eff} \mid H_\beta) + K_{dis}^{em}(T_e^{eff} \mid H_\beta)} \qquad \text{(IV-5)}$$

Similarly, $I_{H\alpha}$ and I_{Q1} ratio is described by:

$$\frac{I_{n\to 2}}{I_{2-2Q1}} = \frac{1}{\eta(T_{gas})} \times \frac{\left(\frac{N_H}{N_{H2}}\right) K_{dir}^{em}(T_e^{eff} \mid H_\alpha) + K_{dis}^{em}(T_e^{eff} \mid H_\alpha)}{A_{a21}^{d^-21} \tau_{d-21} K_{mol}^{ex}(T_e^{eff} \mid Q1)} \qquad \text{(IV-6)}$$

The value K_{dir}^{em} is the rate coefficient for direct excitation, and K_{dis}^{em} is the rate coefficient for dissociative excitation for the listed transition, as dependent on electron temperature, both are enumerated in Table IV-1 [IV-8]. The value $\left(\frac{N_H}{N_{H2}}\right)$ is the atomic to molecular ratio of the hydrogen plasma. The value $A_{a21}^{d^-21} \tau_{d-21} K_{mol}^{ex}(T_e^{eff} \mid Q1)$ is the rate coefficient for the Q1 transition, as dependent on electron temperature. These values have been calculated by Lavrov for a variety of electron temperatures, up to 100 eV. The $\eta(T_{gas})$ term reflects the Q1 emission's dependence on the gas temperature, as the population density of the first rotational level of the ground electronic-vibronic state is noticeably dependent on gas temperature. Its value is given by Lavrov, and represented in Figure (IV-1) [IV-8].

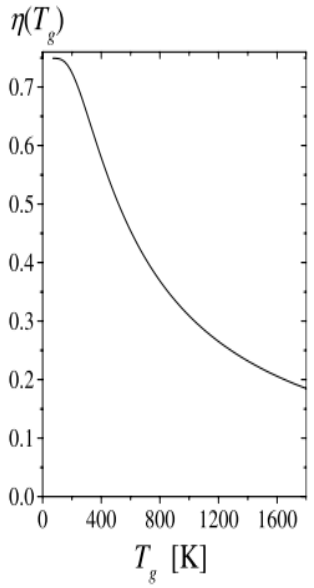

Figure IV-1: The ratio of the population density of the first rotational level of the ground electronic–vibronic state and total density of molecular hydrogen $\eta(T_{gas})$ as used as (IV-6), which is a function of the gas temperature, T_{gas} [IV-8].

Te	Direct Excite K_{dir}^{em}		Dissociative Excite K_{dis}^{em}		K_{mol}^{ex}
eV	H_α	H_β	H_α	H_β	Q1
0.5	4.97E-20	3.93E-21	2.63E-25	2.90E-27	1.06E-22
1	1.15E-14	1.70E-15	5.94E-18	1.10E-19	2.10E-16
1.5	7.03E-13	1.26E-13	1.77E-15	3.65E-17	2.45E-14
2	5.43E-12	1.07E-12	3.06E-14	6.55E-16	2.54E-13
2.5	1.84E-11	3.82E-12	1.69E-13	3.68E-15	1.00E-12
3	4.14E-11	8.86E-12	5.28E-13	1.17E-14	2.46E-12
3.5	7.38E-11	1.61E-11	1.19E-12	2.68E-14	4.58E-12
4	1.14E-10	2.53E-11	2.20E-12	5.03E-14	7.21E-12
4.5	1.60E-10	3.58E-11	3.55E-12	8.26E-14	1.02E-11
5	2.09E-10	4.73E-11	5.21E-12	1.24E-13	1.33E-11
5.5	2.61E-10	5.94E-11	7.15E-12	1.73E-13	1.64E-11
6	3.14E-10	7.19E-11	9.32E-12	2.31E-13	1.94E-11
6.5	3.68E-10	8.45E-11	1.17E-11	2.95E-13	2.22E-11
7	4.21E-10	9.71E-11	1.42E-11	3.65E-13	2.48E-11
7.5	4.74E-10	1.10E-10	1.69E-11	4.42E-13	2.73E-11
8	5.26E-10	1.22E-10	1.96E-11	5.23E-13	2.94E-11
8.5	5.77E-10	1.34E-10	2.24E-11	6.08E-13	3.14E-11
9	6.27E-10	1.46E-10	2.53E-11	6.96E-13	3.32E-11
9.5	6.75E-10	1.57E-10	2.82E-11	7.88E-13	3.47E-11
10	7.22E-10	1.68E-10	3.11E-11	8.81E-13	3.61E-011

Table IV-1: Rate coefficients for the transitions that produce H_α, H_β, and Q1 emission, as calculated by Lavrov, and used in equations(IV-5,6) [IV-8].

Equation (IV-5) can be recast so:

$$\frac{H}{H_2}=\frac{\left(\frac{I_{H\alpha}}{I_{H\beta}}\right)K_{dis}^{em}(T_e|H_\beta)-K_{dis}^{em}(T_e|H_\alpha)}{\left(\frac{I_{H\alpha}}{I_{H\beta}}\right)K_{dir}^{em}(T_e|H_\beta)-K_{dir}^{em}(T_e|H_\alpha)} \tag{IV-7}$$

Likewise, Equation (IV-6) can be recast so:

$$\frac{H}{H_2}=\frac{\left(\frac{I_{H\alpha}}{I_{Q1}}\right)\eta(T_{gas})A_{a21}^{d^-21}\tau_{d-21}K_{mol}^{ex}(T_e^{eff}|Q1)-K_{dis}^{em}(T_e|H_\alpha)}{K_{dir}^{em}(T_e|H_\alpha)} \tag{IV-8}$$

This allows one to plug in the measured intensity ratios, and to plot the atomic to molecular ratio as a function of electron temperature. Where the parameters agree for these two independent ratios yields the parameters for the plasma at that specific state.

At this point it becomes useful to consider the regimes of applicability to the helicon source of the model used. This has also been explored by Lavrov [IV-8], and four plasma parameter regimes have been identified, as illustrated in Figure (IV-2).

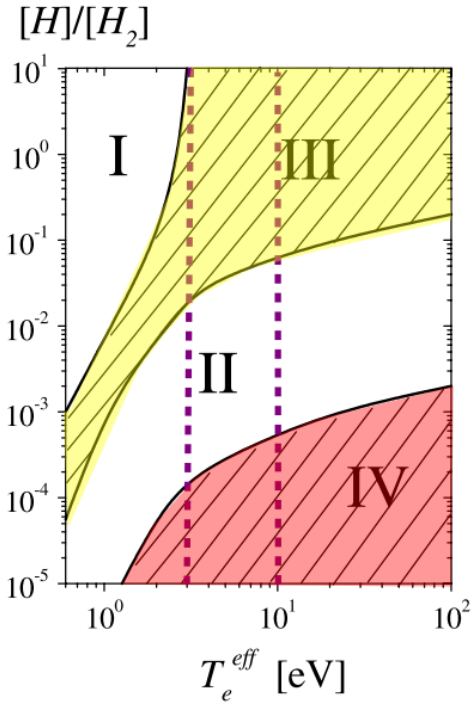

Figure IV- 2: Hydrogen plasma parameter regimes dictate the applicability of the Lavrov CR model as a useful diagnostic tool. The dashed vertical lines are the electron temperature limits for a helicon source plasma [IV-8].

The regimes in Figure IV-2 labeled I and II are regimes where the equations (IV-5) and (IV-6) from chapter IV-B are sensitive to both electron temperature and atomic to molecular species ratio. In regimes I and II both equations (IV-7) and (IV-8) can be applied to precisely diagnose the plasma parameters T_e and atomic to molecular ratio.

In region IV, highlighted in red, equation (IV-5) from chapter IV-B no longer holds, as the $I_{H\alpha}/I_{H\beta}$ intensity ratio is not a function of T_e or the atomic to molecular ratio. However, equation (IV-6) from section IV-B is somewhat applicable, as the $I_{H\alpha}/I_{Q1}$ ratio is sensitive to the atomic to molecular ratio. However, in some cases the intensity ratio exhibits an extreme sensitivity to electron temperature. When in region IV, it is possible to bound the plasma parameters, using equation (IV-8) alone, though the size of those boundaries depends on

where in region IV the plasma exists and how well the electron temperature is known. Previous studies of helicon sources leads to the reasonable bounds for electron temperature being between 3 and 10 eV, as shown in Figure (IV-2) by dashed vertical bars, with 5 eV being the most common electron temperature, even above 3 kW input power.

In region IV, highlighted in red, neither equation (IV-5) nor (IV-6) from chapter IV-B are useful as a diagnostic. The intensity ratios are completely insensitive to electron temperature or atomic to molecular ratio. In this regime physical probes are probably the only recourse for plasma diagnosis.

IV-D) Diagnosis of Electron Temperature and Density

The Fortran source code for Sawada and Fujimoto's hydrogen plasma CR model has been made available by Sawada. The approach taken in using this diagnostic was to generate intensity ratios as dependent on electron temperature and density. Positive diagnosis is considered confirmed when the multiple measured intensity ratios agree with the theoretical intensities, as dependent on electron density and temperature.

As these models are dependent on two variables, multiple intensity ratios must be compared with the model results for agreement to produce a confirmed diagnosis, to show that the model is self consistently in agreement with multiple predictions. This is accomplished when the results agree for multiple intensity ratios. This is also important, as the applicability of this code is not known in advance of application, and agreement of multiple ratios will confirm that the model is accurately describing the observed plasma.

This line intensity ratio is generally described by

$$\frac{I_p(\lambda_{ji})}{I_p(\lambda_{kl})} = \frac{A_{ji} h \nu_{ji} \left(\frac{N_H}{N_{H2}} R_{ji}(H) + R_{ji}(H_2) \right)}{A_{kl} h \nu_{kl} \left(\frac{N_H}{N_{H2}} R_{kl}(H) + R_{kl}(H_2) \right)} \qquad \text{(IV-9)}$$

where I_p is the photon count rate, A_{yx} is the Einstein spontaneous emission coefficient for the y to x transition, h is Planck's constant and ν_{yx} is the frequency of the relevant transition, $\frac{N_H}{N_{H2}}$ is the atomic to molecular hydrogen ratio, $R_{yx}(H)$ is the population-rate coefficient for the y to x level for atomic hydrogen, and $R_{yx}(H_2)$ is the population-rate coefficient for the y to x level for molecular hydrogen.

Sawada's code provides the rate coefficients for a variety of electron density and temperatures, and N_H/N_{H2} ratio is determined earlier. Using the N_H/N_{H2} ratio, agreement with the observed plasma intensity ratios and the intensity ratios predicted by Equation (IV-9) yields the electron population characteristics.

References for Chapter IV

IV-1 D. Schieber, S. Gavril, and MS Erlicki, "Electron temperature determination in a low density helium plasma," Plasma Physics 12.11 (1970): 897-9.

IV-2 RF Boivin, JL Kline, and EE Scime, "Electron temperature measurement by a helium line intensity ratio method in helicon plasmas," Physics of Plasmas 8 (2001): 5303.

IV-3 T. Shikama, et al, "Molecular Zeeman spectroscopy for H Fulcher-α band spectra as a local measurement of rovibrational structures," Physics of Plasmas 14 (2007): 072509.

IV-4 J. Vlcek and V. Pelikan, "A collisional-radiative model applicable to argon discharge over a wide range of conditions. IV. Application to inductively coupled plasmas," Journal of Physics D: Applied Physics 24.3 (1991): 309-17.

IV-5 K. Kano, M. Suzuki, and H. Akatsuka, "Spectroscopic measurement of electron temperature and density in argon plasmas based on collisional-radiative model," Plasma Sources Sci.Technol 9 (2000): 314-22.

IV-6 J. Vlcek and V. Pelikan, "A collisional-radiative model applicable to argon discharges over a wide range of conditions. II. Application to low-pressure, hollow-cathode arc and low-pressure glow discharges," Journal of Physics D: Applied Physics 22 (1989): 632-43.

IV-7 X. M. Zhu and Y. K. Pu, "A simple collisional radiative model for low-pressure argon discharges," Journal of Physics D: Applied Physics 40.8 (2007): 2533-8.

IV-8 B. P. Lavrov, A. V. Pipa, and J. Ropcke, "On determination of the degree of dissociation of hydrogen in non-equilibrium plasmas by means of emission spectroscopy: I. The collision-radiative model and numerical experiments," Plasma Sources Science & Technology 15.1 (2006): 135-46.

IV-9 T. Fujimoto, S. Miyachi, and K. Sawada, "New density diagnostic method based on emission line intensity ratio of neutral hydrogen in an ionizing phase plasma," Nuclear Fusion 28.7 (1988): 1255-63.

IV-10 T. Fujimoto, K. Sawada, and K. Takahata, "Ratio of Balmer line intensities resulting from dissociative excitation of molecular hydrogen in an ionizing plasma," Journal of Applied Physics 66 (1989): 2315.

IV-11 K. Sawada, K. Eriguchi, and T. Fujimoto, "Hydrogen-atom spectroscopy of the ionizing plasma containing molecular hydrogen: Line intensities and ionization rate," Journal of Applied Physics 73 (1993): 8122.

IV-12 K. Sawada and T. Fujimoto, "Effective ionization and dissociation rate coefficients of molecular hydrogen in plasma," Journal of Applied Physics 78 (1995): 2913.

V-A) Overview of Helicon Source Background and Theory - Introduction

The plasma source diagnosed in this work is a helicon source. This high efficiency, high density plasma source, a brief review of its history, and some applications of this device have already been described in Chapter II. This section will first give a brief review of the state of helicon source theory to date. However, this thesis is focused on helicon source diagnosis, not development or physics, so the reader will have to refer to the referenced literature for a more complete treatment of the operation and understanding of the helicon source.

Once basic helicon source theory has been established, progress in helicon source diagnostics will be discussed. This will begin with the state of the art in probe diagnostics as applied to helicon source plasmas, and then optical diagnostics as applied to helicon source plasmas.

V-B) Helicon Source Theory and Operation

The dispersion relation for a helicon wave is that of a whistler wave confined to a cylinder with a coaxial magnetic field, sometimes referred to as a bound whistler wave. These waves have a frequency between the ion and electron cyclotron frequencies. Such a wave is governed by the dispersion relation

$$k \nabla \times B = k_w^2 B \qquad \text{(V-1)}$$

$$\nabla^2 B + \alpha^2 B = 0 \qquad \text{(V-2)}$$

where k_w is the wave number for the low frequency whistler wave propagated along the magnetic field

$$k_w^2 \equiv \frac{\omega \omega_p^2}{\omega_c c^2} = \frac{\omega n_o e \mu_o}{B_o} \qquad \text{(V-3)}$$

where, B_o is the magnetic field in free space, k is the axial-wave number, α is the boundary parameter $\frac{k_w^2}{k} = \alpha$, ω_c is the electron cyclotron frequency, ω_p is the plasma frequency for a plasma of density n_o, e is the electron charge, and μ_o is the permeability of free space. The components of the magnetic field may be solved in a cylindrical coordinate system, producing a sum of J type Bessel functions [V-1].

The dispersion relation of the helicon wave in the simple case has been solved, though it is not a trivial exercise even under ideal conditions. The system's dispersion relation becomes more complicated when taking into account nonuniform density profile and magnetic field. Further, there are a variety of observed phenomena exhibited in helicon sources that the theory supporting helicon source development cannot yet account for [V-2]. The reason that the helicon source is an efficient plasma source is not well understood.

For some time it has been hypothesized that a helicon mode produces a non-Maxwellian electron population via Landau damping [V-3]. Two other competing theories accounting for the high efficiency of the helicon source are the existence of Trivelpiece-Gould (TG) waves and lower hybrid wave coupling[V-4].

Due to the parallel phase velocity of a helicon wave matching electron thermal

velocities in the 20-200 eV range, it was thought that helicon waves were particularly suited to making a high energy electron population distribution that would be efficient ionizers. However, this has not been born out in experiment despite numerous attempts to detect the presence of a high energy electron population tail. In fact, the most carefully executed diagnostics using RF compensated probes showed a Maxwellian electron energy distribution[V-3,5]. Yet at densities below 10^{12} cm^{-3} there is evidence that the electron energies pulse at the RF frequency, indicating some wave-particle interactions at low density. Regardless, studies have concluded that CR modeling, assuming a Maxwellian electron energy distribution, can be applied as a diagnostic in helicon source plasmas with confidence [V-6].

The TG waves, if they play a significant role, exist at the non-conducting boundaries of the plasma, where a strongly damped 'slow mode' wave is superimposed on the weakly damped helicon wave. This slow mode damps quickly and is present in a very small volume of the helicon source, making its existence difficult to experimentally verify.

The theory hypothesizing that the helicon wave has resonant coupling with the lower hybrid wave, producing superior ionization, is supported in the observed ion temperature and plasma density peaking near this lower hybrid frequency. In addition, self-consistent codes that predict that the plasma resistance is highest at the lower hybrid frequencies.

While these theories all have their merits, none have shown clear superiority to the rest. Helicon source theory will progress, as the operational understanding of the devices improves and continues to inform the theory.

V-C) Previous Helicon Source Diagnostic Work

The helicon source is a high temperature high density plasma source that generates plasma through a combination of RF and magnetic fields; for these reasons the helicon source is a difficult device to diagnose. The RF can induce a variety of effects in physical probes that make diagnosis more difficult than when used in diagnosing plasmas generated by other means [V-7,8]. Further, the magnetic fields in a helicon source can produce localized increased ion density making ion density readings difficult. The high ion density and temperature common in a helicon source plasma can melt or vaporize physical probes [V-9], and will typically sputter a probe [V-10]. This contaminates the plasma and produces inconsistent probe readings that can be detrimental to both helicon source utilization and diagnostics. Probe survival can be achieved if the helicon source measurements are made in short duration discharges [V-11]

In the 90's there was some success in obtaining helicon source electron temperature and density measurements, using sophisticated RF compensated probes [V-12, 13]. Probe RF compensation can be achieved in a variety of ways. The simplest method is passive compensation, that utilizes a filter circuit to reject the 1st harmonic of the RF frequency driving the plasma, however this neglects the noise that higher harmonics can generate in the probe signals. Another method utilized is to apply an attenuated phase shifted bias from the RF generator to a probe signal, to achieve the maximum positive floating potential, which again can only compensate the 1st harmonic of noise produced by the RF driving the plasma but has the advantage of referencing the plasma conditions, not the driving generator [V-14].

A more sophisticated method of compensating a probe in a RF plasma is to couple the powered probe to a floating probe through a large capacitor where the floating probe is placed close to the powered probe[V-12]. Due to the coupling between the probes at the probe site, the lowest two harmonics are effectively compensated. This method has successfully diagnosed reactive ion etching plasmas as well as high density and temperature helicon source plasmas.

In helicon sources, this compensated probe technique has successfully diagnosed helicon source plasma electron temperature and plasma density, parameterizing the helicon source plasma response to RF power, magnetic field, and the change in plasma density as a function of radial position in the helicon source tube. These methods have produced a more accurate plasma diagnostic of the helicon source plasma, measuring electron temperatures a few eV lower than indicated by uncompensated probes.

Campaigns to use probes for helicon source plasma diagnosis have been very useful in giving an accurate plasma diagnosis, used in vetting theory as well as parameterizing helicon source operation. These probe campaigns have successfully achieved a series of localized diagnoses to produce a high fidelity mapping of helicon source plasma profiles, which has been very important to helicon source theory work, as the nonuniform profile introduces a variety of complications in helicon wave propagation.

Carbon probes have been successfully used to minimize the sputtering of the probe in the abrasive environment, however the non-uniformity in measurement over time due to erosion and plasma impurities cannot be eliminated. For this reason, an ideal plasma diagnostic should be remote.

In principle, a double probe system constructed of carbon combines the advantages of robustness in the plasma environment and RF compensation. Survivability of these probes remains an open question in application. Such probes in fact have survived the plasmas of the conditions typically generated by helicon sources in hydrogen. One concern is a probe intersecting a magnetic field line may see an elevated electron flux that perturbs the readings of the probe, and may even represent a threat to the probe survivability.

A CR diagnostic will have a variety of advantages if an average electron temperature and density measurement is a sufficient diagnosis and there is a CR model that applies to the plasma operation regime. In the instance that it is unsuitable to consider a plasma as an average body, an Abel inversion must be used with readings of cords across the plasma to get a proper sense of the plasma profile. This diagnostic approach, treating the plasma as an average body, has been successfully performed in a variety of campaigns with the majority of work done in argon discharges [V-15,16,], as well as helium [V-10,17]. The application of the CR diagnosis technique in a helicon source hydrogen plasma has been done only recently [V-18,19,20,21]. While these studies have achieved a successful diagnosis, most publications have not addressed the regimes for which this method is effective. As a result, it is necessary in application to check that the CR model used is an adequate model of the plasma under study.

References of Chapter V

V-1 F. F. Chen, "Generalized theory of helicon waves. I. Normal modes," Physics of Plasmas 4.9 (1997): 3411.

V-2 HD Jung, et al, "Development of a compact helicon ion source for neutron generators," Review of scientific instruments 75.5 (2004): 1878-80.

V-3 FF Chen and RW Boswell, "Helicons-the past decade," Plasma Science, IEEE Transactions on 25.6 (1997): 1245-57.

V-4 C. M. Franck, Experiments on Whistler Wave Dispersion in Bounded Magnetised Plasmas s. n, 2003).

V-5 F. F. Chen and D. D. Blackwell, "Upper Limit to Landau Damping in Helicon Discharges," Physical Review Letters 82.13 (1999): 2677-80.

V-6 RF Boivin, JL Kline, and EE Scime, "Electron temperature measurement by a helium line intensity ratio method in helicon plasmas," Physics of Plasmas 8 (2001): 5303.

V-7 VA Godyak, RB Piejak, and BM Alexandrovich, "Probe diagnostics of non-Maxwellian plasmas," Journal of Applied Physics 73 (1993): 3657.

V-8 A. Garscadden and KG Emeleus, "Notes on the Effect of Noise on Langmuir Probe Characteristics," Proceedings of the Physical Society 79.3 (1962): 535-41.

V-9 G. R. Piefer, Performance of a Low-Pressure, Helicon Driven IEC 3He Fusion Device, Ph.D. Nuclear Engineering and Engineering Physics, University of Wisconsin - Madison, 2006.

V-10 RF Boivin, JL Kline, and EE Scime, "Electron temperature measurement by a helium line intensity ratio method in helicon plasmas," Physics of Plasmas 8 (2001): 5303.

V-11 Gilland. J H, , PhD (Nuclear Engineering and Engineering Physics), University of Wisconsin - Madison, 2004.

V-12 I. D. Sudit and F. F. Chen, "RF compensated probes for high-density discharges," Plasma Sources Science and Technology 3.2 (1994): 162-8.

V-13 SN Ghosh, et al, "Study of High-Density Helicon-Plasma Generation and Measurement of the Plasma Parameters by Using a Frequency-Compensated Langmuir Probe," Journal of the Korean Physical Society 48.5 (2006): 908-13.

V-14 N. S. J. Braithwaite, NMP Benjamin, and JE Allen, "An electrostatic probe technique for RF plasma," Unknown (1986).

V-15 X. M. Zhu and Y. K. Pu, "A simple collisional radiative model for low-pressure argon discharges," Journal of Physics D: Applied Physics 40.8 (2007): 2533-8.

V-16 J. Vleck, "A collisional-radiative model applicable to argon discharges over a wide range of conditions. I. Formulation and basic data," J. Phys. D: Appl. Phys. 22 (1989): 623-31.

V-17 S. Sasaki, et al, "Helium I line intensity ratios in a plasma for the diagnostics of fusion edge plasmas," Review of Scientific Instruments 67 (1996): 3521.

V-18 M. Goto, K. Sawada, and T. Fujimoto, "Relations between the ionization or recombination flux and the emission radiation for hydrogen and helium in plasma," Physics of Plasmas 9 (2002): 4316.

V-19 MD Carter, et al, "Comparing experiments with modeling for light ion helicon plasma sources," Physics of Plasmas 9 (2002): 5097.

V-20 M. Goto, et al, "Determination of the hydrogen and helium ion densities in the initial and final stages of a plasma in the Large Helical Device by optical spectroscopy," Physics of Plasmas 10 (2003): 1402.

V-21 EM Sciamma, et al, "Spectroscopic Electron Temperature Measurement of the Recombining Plasma on the VASIMR Experiment," Presented at the 30th International Electric Propulsion Conference IEPC-2007-185 (2007).

VI-A) Experimental Setup and Technique – Introduction

To begin with, this chapter will briefly describe spectrometer theory and nomenclature. Once the theory has been established, the specifics of the spectrometer used in this work will be described. Also the usage of the spectrometer will be explored. Finally, the helicon source diagnosed in this work will be described.

VI-B) Spectrometer Design and Theory

The diffraction grating spectrometer is an apparatus that separates polychromatic light into its monochromatic constituents. There are various types of spectrometers, however the diffraction grating spectrometer has had the most development in recent years due to its ease of instrumentation and usefulness as a method to separate light by changing the spatial modulation of the refractive index without absorption seen in transmission diffraction.

The first diffraction grating was made in the late 18^{th} century, but it was not until 1821 that Joseph von Fraunhofer truly examined the diffraction grating and utilized it as a scientific apparatus, allowing him to identify Fraunhofer lines, the spectral absorption lines observed in the Sun. Development of this technology continued throughout the 19^{th} century, and by the 20^{th} century it had become the dominant method of spectroscopic analysis.

The diffraction grating profile is a series of parallel surfaces, typically referred to as grooves, so incident beams are separated by the grooves into distinct wavefronts. These wavefronts are closely and regularly spaced so that the wavefronts are in phase and interact

to produce interference. The dispersion of this interference depends on the path length of the wavefronts. The diffraction grating is, in the simple ideal case, ruled by the grating equation, equation (VI-1):

$$\frac{m\lambda}{d} = \sin(\alpha) + \sin(\beta_n) \qquad \text{(VI-1)}$$

where m is the order of reflection (an integer value), λ is the wavelength of the photon, d is the distance between grooves (1/d is known as G, the groove density), α is the angle of incidence to the normal, and β is the angle of reflection to the normal [VI-1]. These angles of incidence and reflection are measured from the normal plane of the grating, as is illustrated in Figure VI-1. It should be noted that for each order of reflection (m), there are multiple angles of reflection ($\beta_{0,\pm1,\pm2,\pm3\ldots}$).

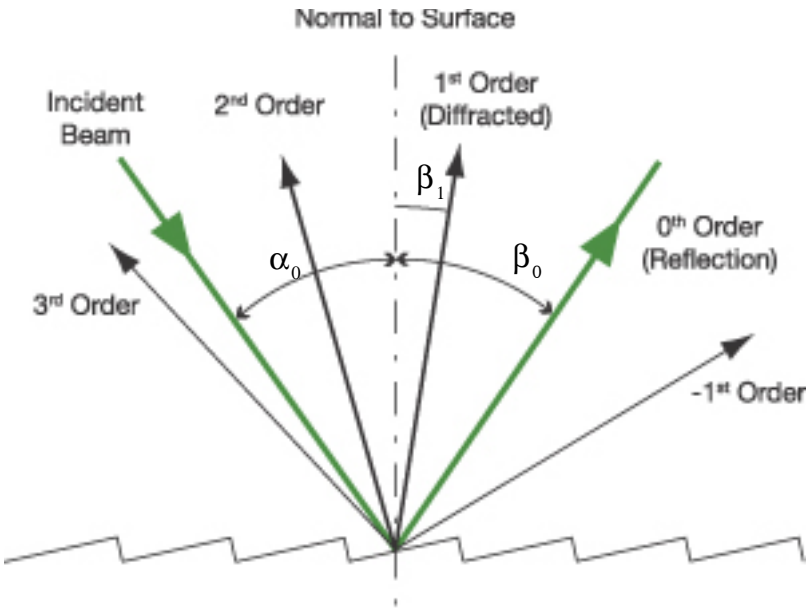

Figure VI-1: Schematic representation of rays traveling to a diffraction grating and the multiple orders of reflections that are produced [VI-1].

There are also transmission gratings, which are governed by the same grating equation, though they depend on refraction rather than reflection to produce the diffraction. Principally these gratings produce the same results, but transmission can lead to aberrations that must be dealt with, and it is important to know the transmission characteristics of the transmission grating media. For these reasons reflection gratings are preferred.

Examination of the grating equation shows that only the orders where $\left|\frac{m\lambda}{d}\right| < 2$ are allowed. Reflection of the order 0 is always allowed, this is called specular reflection. Specular reflection is useless to spectroscopy, as all wavelengths follow the same angle, and cannot be distinguished. Also, both the positive and negative of an allowed order are always present.

It is also important to note that overlap of dispersion is allowed, that is the light from different orders can occupy the same projection space. This can lead to confusion, as detectors typically measure intensity, and can not tell when the low end of one order overlays the high end of another. Care must be taken in the design and use of the spectrometer so that across the measured bandwidth the paths can diverge enough that the orders do not overlap on the plane of the detector.

While the grating equation is insensitive to the angle from the normal to the reflection surface, this 'blaze angle' does impact the energy distribution of the reflected light. A grating is most efficient when the blaze condition is met

$$m\lambda_b = 2d\sin(q_b) \qquad \text{(VI-2)}$$

where λ_b is the blaze wavelength (the wavelength the diffraction grating is designed to

optimally perform), and q_b is the blaze angle of the grating. When the blaze condition is met the incident and diffracted rays follow the have equal incident and reflected angles, as seen from the reflecting surfaces. This allows for the refraction grating to be optimized for a specific region of a spectrum and for a specified order. This makes diffraction gratings valuable, as the wasted power in the 0^{th} order reflection is reduced, and the power in a more useful order of reflection is increased.

VI-C) Spectrometer Model and Characteristics

The spectrometer used in this study is the Newport Oriel LineSpec, illustrated as a schematic in Figure VI-2, with charge-coupled device (CCD) detector. This is a relatively low cost spectrometer that provides a wide variety of operating conditions as components are modular and can be swapped to match the needs of the application[VI-2]. It is a Czerny-Turner configuration spectrometer, with two spherical mirrors and a planar diffraction grating, producing a flattened spectral field and reasonable coma correction, though some spherical aberration and astigmatism remain. The three important tradeable elements internal to the LineSpec spectrometer are input slit width, diffraction grating, and detector. The spectrometer is coupled to a coaxial cable which is connected to a light gathering optic. The LineSpec's performance depends on the hardware chosen and software settings.

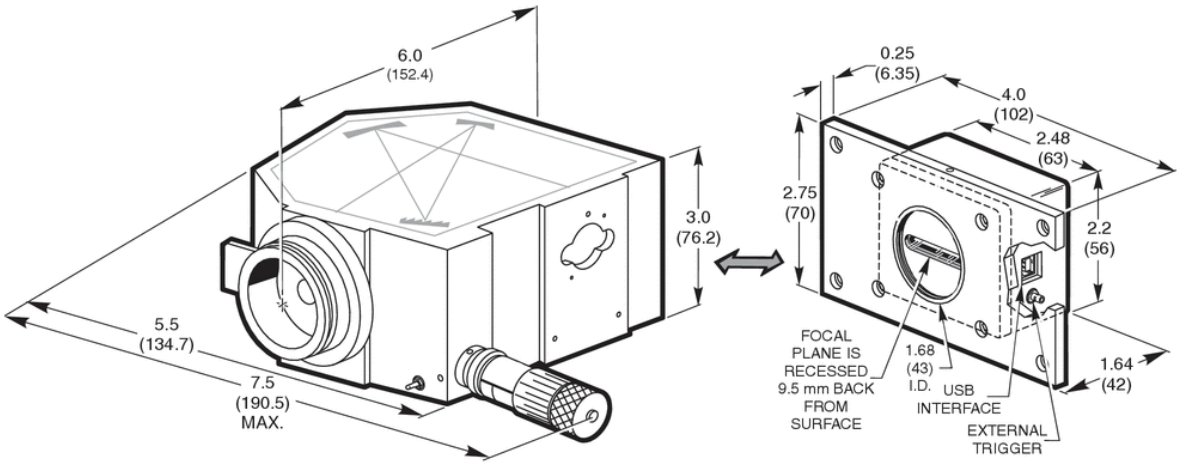

Figure VI- 2: Schematic of the LineSpec spectrometer [VI-2].

The device accepts a variety of input slits, sold by Newport, between 10 and 200 µm wide, allowing for optimization of signal strength and resolution. These are fixed width slits, rather than a knife edge, which would provide more tunability of that component. These slits are 3 mm tall, except the 10 µm wide slit which is 2 mm tall. In the helicon source under study, the plasma source is bright, and the light gathering optics are large enough, so the 10 µm wide slit can be used for the diffraction slit, allowing the highest possible resolution for that component. Measurement of dimmer sources may necessitate the use of wider entrance slits to provide increased signal strength, though the full width half maximum (FWHM) will be increased and subsequently the resolution will be decreased, as illustrated in Figure VI-3.

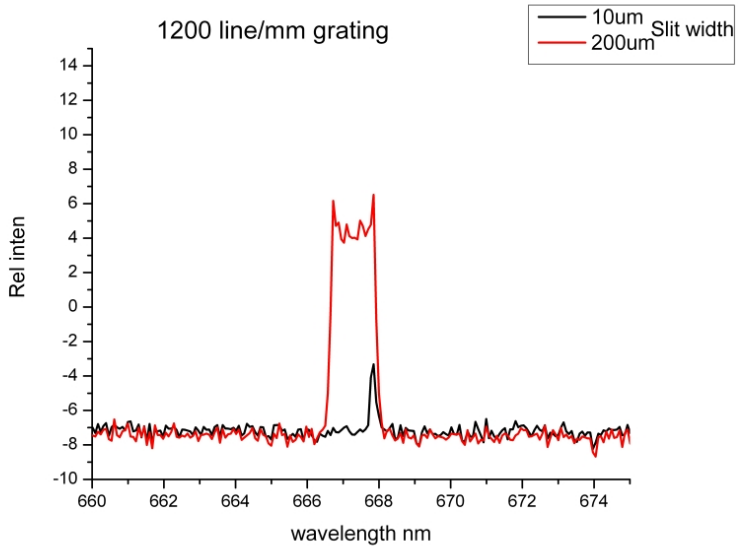

Figure VI- 3: A comparison of the spectrometer response to a difference in inlet slit with all other parameters held equal while observing a hydrogen discharge lamp. Note, the 200 μm slit actually does not produce a Lorentz profile, but a projection of the slit.

The spectrometer also utilizes a variety of gratings depending on the required bandwidth under study and resolution required. The more fine the grating ruling the higher resolution the spectrometer will produce (all other things being equal), but the more narrow the measured spectrum will be. Newport makes both ruled and holographic diffraction gratings that are comparable in performance. The spectrum produced is tunable via a micrometer drive, that turns the grating to tune to a portion of bandpass projected onto the light detector array. A 1200 l/mm diffraction grating was used in this study, as it accommodated the wavelength range required and and provided the resolution necessary to distinguish relatively closely spaced molecular lines.

In the utilized setup the light measurement is made by a CCD detector. The listed spectral response of the CCD is 200-1000 nm, with 2048 active pixels in an array that is 28

mm wide. The device takes an exposure between 8 ms and 10 s, allowing for optimization of light gathering time and noise. The device is not cooled, which makes it more susceptible to thermal noise, but included in the LineSpec package is software that can perform averaging over a series of exposures to reduce random noise. The CCD detector was chosen over a complementary metal–oxide–semiconductor (CMOS) detector, as the CCD provides a higher resolution and greater dynamic range. However, the CCD performs with a lower quantum efficiency, as illustrated in Figure VI-4.

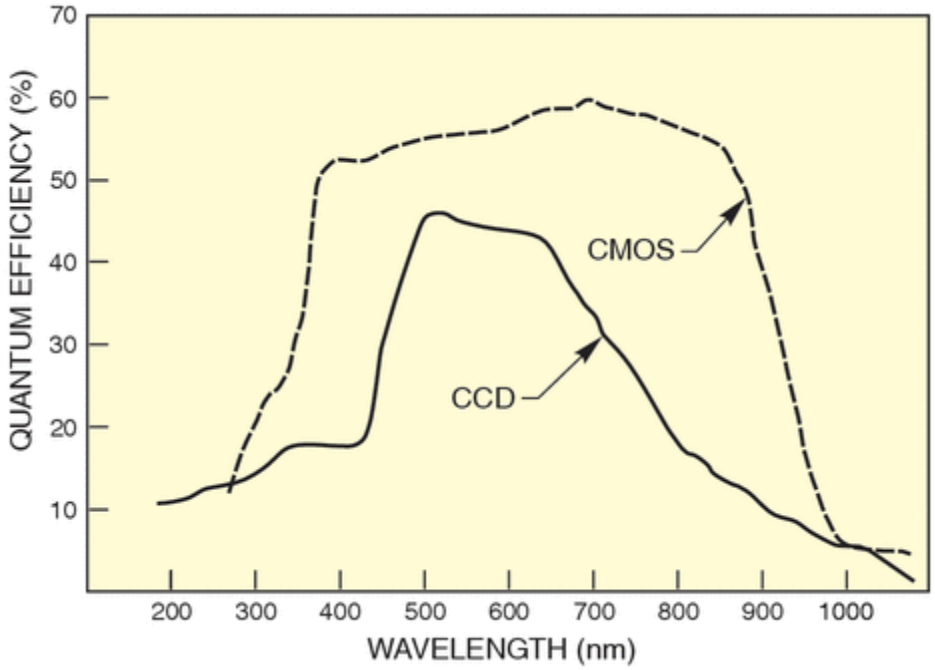

Figure VI- 4: The quantum efficiency of the detectors available for the LineSpec spectrometer [VI-5].

The optic used to couple light into the coaxial cable has an effectiveness based largely on geometric optics principles. The etendue (the measure of light accepted into a series of irises) of a fiber-optic is notoriously low, but it is unparalleled for transmission of light. A large lens properly focused on the fiber-optic end optimizes the light gathering ability of the

system.

The system used in this study is described by the maker as having a blaze wavelength of 500 nm, with a peak efficiency of 80% [VI-3]. The spectral resolution is 0.22 nm, with an array bandpass of 170 nm. The exposure time typically used was 1.0 s.

Because the diffraction grating is tunable, wavelength calibration must be performed when the grating is changed or the grating tuning is altered. This was proformed using plasma discharge lamps, primarily hydrogen and helium discharges. A proper calibration requires three identified wavelengths correlated to three pixels on the CCD. Helium was the most valuable in this, as helium exhibits three strong lines across the pertinent bandwidth. The measured spectra were compared with the reference spectra produced by the National Institute of Standards and Technology (NIST)[VI-4]. The calibration was then checked against the hydrogen discharge lamp and associated NIST reference spectra.

To determine absolute intensities of lines it is necessary to measure a lamp with a standardized spectrum, usually a standardized tungsten filament lamp. However, this is not required if comparisons of relative intensity are all that is needed.

Comparing the relative intensity of lines is possible, so long as the spectrometer's wavelength response is known (and the rest of the system is largely wavelength insensitive across the bandwidth of interest). The spectrometer's wavelength response is determined by the CCD's quantum efficiency, as provided by the manufacturer, and shown in Table VI-1 [VI-5].

Line	**Wavelength [nm]**	**Quantum Efficiency [%]**
Balmer H_β	486.1	42.3
Balmer H_γ	434.0	19.4
Balmer H_δ	410.2	17.9
Q1 molecular line	622.5	43.7

Table VI-1: Quantum efficiency for wavelengths relevent to Hydrogen plasma for the CCD used in this campaign [VI-5].

The measured signal strengths are described by

$$S_{\lambda-measured} \propto QE_{\lambda} S_{\lambda-absolute} \tag{VI-3}$$

where the S designates signal strength and QE_λ designates the CCD quantum efficiency for that wavelength. Aside from the quantum efficiency, the system response to all wavelengths may be largely considered constant.

Measured signal strengths are scaled to a reference quantum efficiency to produce a normalized signal strength, in this case the H_α line at 656.3 nm.

$$S_{b-measured}\left(\frac{QE_a}{QE_b}\right) = S_{b-scaled} \tag{VI-4}$$

When the relevant measured signals are all on the same scale, true signal ratios can be taken. However, these signal ratios are not intensity ratios, and intensity is required for data analysis. An intensity is measured in energy, which a CCD cannot measure. A CCD effectively counts photons; when a photon hits a pixel a charge is liberated and stored in the pixel until the pixel is read.

Because the spectrometer splits the spectrum, it is valuable to convert the signal to an intensity with respect to a reference signal, in this case the H_α signal. To convert the scaled signal into a scaled intensity one must use the formula

$$S_{scaled}\left(\frac{hc}{\lambda}\right)=I_{scaled} \tag{VI-5}$$

where h is Planck's constant, c is the speed of light, λ is wavelength, and I is relative intensity. So long as the wavelength units are consistent, the units of intensity will be consistent when ratios are taken and cancel out.

VI-D) Helicon Source Design and Operation

The helicon source used was designed as an ion source for an inertial electrostatic confinement (IEC) device. The helicon source was built by Dr. Gregory Piefer at the University of Wisconsin for the Fusion Technology Institute Inertial Electrostatic Confinement Fusion Laboratory Advanced Fuels Project. The helicon source is utilized on the HELIOS IEC device at the University of Wisconsin Advanced Fusion Fuels Project [VI-6], and presented in Figure VI-6, and pictured in operation in Figure VI-7.

The helicon source plasma is produced in a tube with a 52 mm inner diameter, with 2 mm thick quartz walls, and a total length of about 44 cm. Quartz was chosen for superior thermal properties, tolerance for extreme temperature gradients and low thermal expansion properties. Quartz is also ideal for light transmission, as quartz has very low absorption across the visual band with even transmission, as seen in Figure VI-5, making correction of observed spectra much simpler [VI-7].

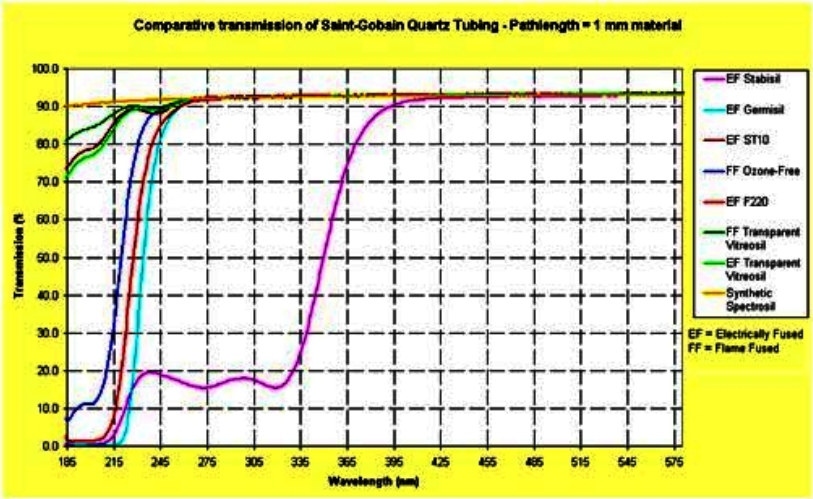

Figure VI- 5: Transmission curves for a variety of types of quartz as provided by Saint-Gobain. The transmission remains flat for all materials listed, up to 2000 nm [VI-7].

The quartz tube is sealed on both ends by o-ring compression seals. The inlet cap has a 6 mm Swagelok fitting for coupling to a gas manifold. The outlet cap is fitted to a stainless steel coupler that is mated to the low pressure IEC device chamber. These inlet and outlet caps have copper water cooling lines for heat rejection as the caps and components do not have the heat resistance of the quartz. The heat load on the outlet end is particularly high as the plasma exits the helicon source through an orifice into the IEC chamber. Because this heat load at the outlet is so high, the o-ring there is made of Kalrez perflouroelastomer, and the extraction side o-ring is shielded by a castable alumina ceramic shield to prevent the melting of the o-ring. The inlet end o-ring is composed of Viton rubber.

The quartz tube is inside an antenna built to launch helical waves, in this case a Nagoya III type antenna. The construction is of 6 mm copper tubing, through which water cooling is flowed, as kW's of RF power is removed through it. The rear lead of the antenna is coupled to the RF power supply through a matching circuit, and the front is connected to

ground. The supply operates on the standard 13.56 MHz. Water cooling was necessary due to the small antenna size causing low radiation resistance and requiring a high current, which produces a high resistive heating.

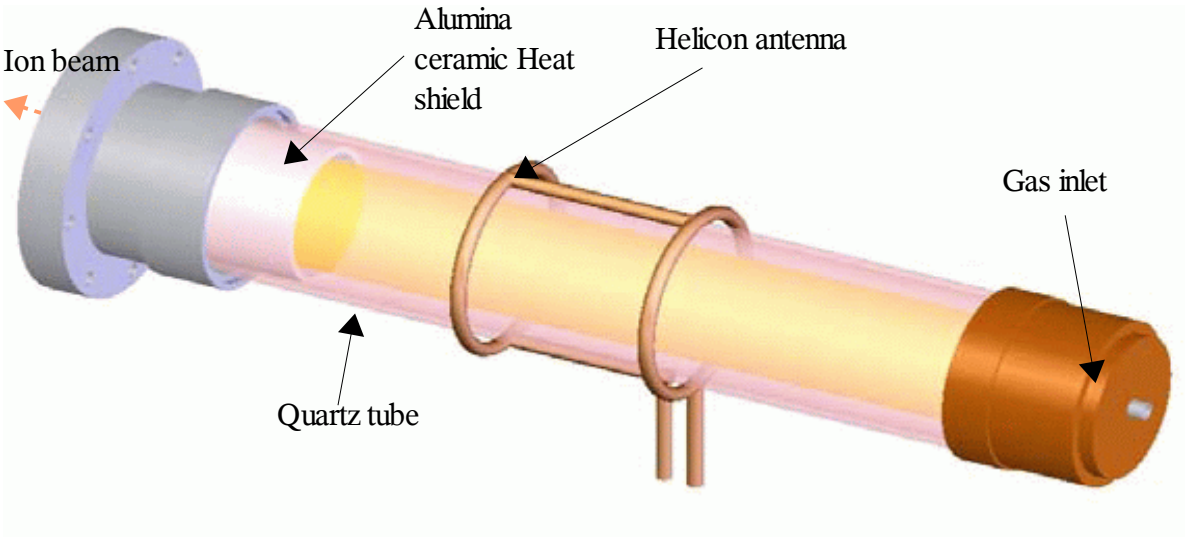

Figure VI-6: A schematic of the UW IEC helicon ion source. Pictured are a diagram of the quartz tube, end caps, ceramic heat shield (white), and helicon antenna[VI-6].

The matching circuit used is a 'type L' which keeps the impedance at Z= 50+0j Ω. The current load was high through this component as well, requiring water cooling.

Two power supplies were used during this campaign. The first was a loaned Comdel CPS 3000 RF power supply. This supply was replaced by an Advanced Energies RFG 3000 Generator. Both supplies are water cooled. Both supplies are capable of providing up to 3 kW of RF power, but for this work the system never exceeded 2 kW, as the Kalrez o-ring on the outlet end cannot withstand the resultant power extremes.

The magnetic field was provided by a water cooled Varian commercial electromagnet pair, which is enclosed in a ferritic cage to reduce fringing fields. The magnets produce from $< 1x10^{-5}$ to 2 T.

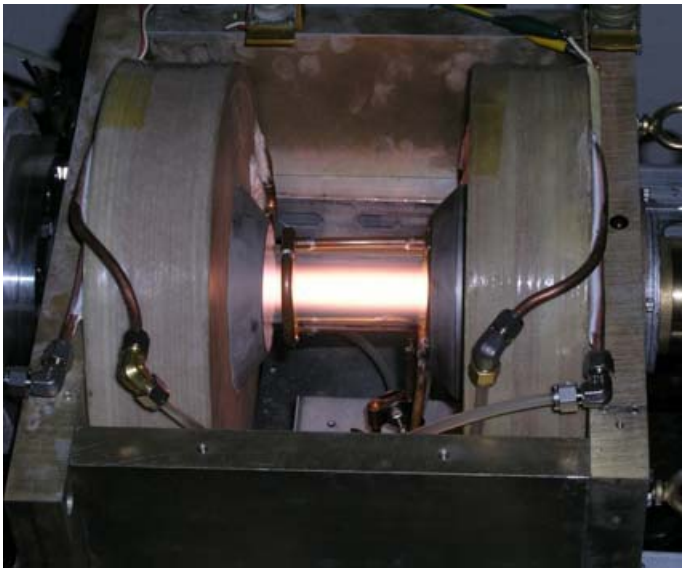

Figure VI- 7: A top view picture of the helicon source in operation.

The helicon source, as currently configured, has produced at a maximum 30 mA deuterium ion current at 1800 W and 0.11 T [VI-8]. Attempts to directly diagnose the plasma inside the helicon source have proved impossible at high power, as all physical probes have melted in the energetic plasma environment. Due to probe survivability difficulties, a direct measurement of the plasma density and electron temperature was not made, and inference from comparison to other helicon sources provides only an estimate of the plasma conditions. It is difficult to know if the helicon source should be able to produce more than a 30 mA ion current due to the lack of direct diagnosis, though theory suggests it is likely.

References for Chapter VI

VI-1 C. Palmer, "Diffraction Grating Handbook," Richardson Grating Laboratory, Rochester, NY (2005).

VI-2 “Image – 881.gif”, Newport Corp. 7/12/2008 <http://www.newport.com/images/webclickthru-EN/images/881.gif>.

VI-3 Oriel LineSpec User's Guide, 2006, Newport Inc.

VI-4 NIST Atomic Spectra Database Lines Form, 11/8/2007 <http://physics.nist.gov/PhysRefData/ASD/lines_form.html>.

VI-5 Image - 879, 2/10/2008 <http://www.newport.com/images/webclickthru-EN/images/879.gif>.

VI-6 G. R. Piefer, Performance of a Low-Pressure, Helicon Driven IEC 3He Fusion Device, UW Madison, PhD dissertation. December, 2006).

VI-7 Saint-Gobain, "Comparative transmission of Saint-Gobain Quartz-tubing - pathlength = 1mm material," 2007 Abstract.

VI-8 S Zenobia, data from Helios run 303, (9/13/2007)

VII-A) Results – Introduction

The Results of the helicon source diagnosis campaign are listed here. First, the results of the helicon source gas temperature measurement method outlined in Chapter III-B are laid out, starting with a brief examination of the molecular line data that produces the helicon source gas temperature. These results will allow for the derivation of the gas pressure and density inside the helicon source during operation, as outlined in Chapter III-C.

The hydrogen atomic to molecular density ratio results are produced next, using the method outlined in Chapter IV-C. This section begins with recasting some of the results done by Lavrov [VII-1], and then producing the atomic to molecular density ratios obtained from these results.

The next section will examine the electron population temperature and density. First matrices of rate coefficients produced by Sawada's CR model, discussed in Chapter IV-D, will be produced. Application of these rate coefficients and the obtained atomic to molecular density correlated against observed emission ratios produce, in some cases, a measurement of the electron temperature and density.

VII-B) helicon source Gas Temperature Diagnosis

Observation of molecular lines in the helicon source has consistently yielded reasonable results. The method by which this diagnosis was made was discussed exhaustively in Chapter III-B. The 1996 study by Astashkevich, et al. provides the necessary constants to perform this diagnosis [VII-2]. From these available coefficients, a set of lines with a common (n', v') was chosen to perform a spectroscopic rotational temperature

diagnosis, as illustrated in Figure VII-1. Due to overlapping spectra, it can be difficult to find a useful set of emission lines that have readily distinguishable intensity peaks.

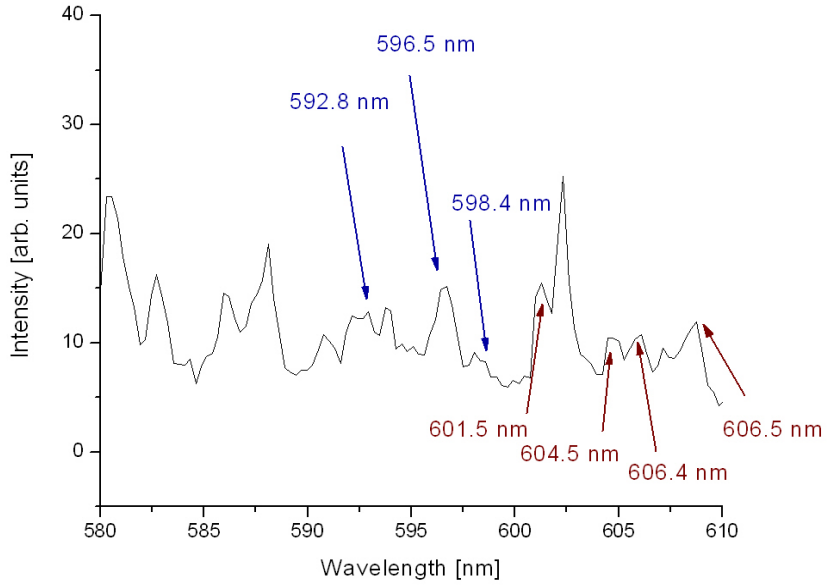

Figure VII-1: An example of molecular lines observed in the helicon source. The profile and structure in this range remained relatively consistent throughout the operating parameter space of the helicon source. The v=1 lines are labeled in red, and the v=2 lines are labeled in blue.

The observed emission is illustrated in Figure VII-1, listing the wavelength predicted by Astashkevich, and the observed wavelength. While the noise in the results at this intensity scale might raise some concern, the repeatability of the spectrum profile leads us to believe that the averaging routine performed by the spectrometer does an adequate job of mitigating thermal noise. With the observed intensities and the atomic data assembled by Astashkevich, we can then apply equation (II-5), re-expressed here:

$$\ln\left(\frac{I^{n',v',N'}_{n'',v'',N''}}{A^{n',v',N'}_{n'',v'',N''}\, g_{a,s}(2N'+1)}\right)=\ln(C)-\frac{hcE_{n',v',N'}}{kT_{rotational}(n',v')} \qquad \text{(VII-1)}$$

Producing plots utilizing v'=1 and v'=2 transitions:

Repeating this analysis across operation space allows for a parameterization of the helicon source gas temperature. An example of this analysis is illustrated for the Q branches of the $(i^3\Pi_g^-, v=1)\rightarrow(c^3\Pi_u, v=1)$ and $(i^3\Pi_g^-, v=2)\rightarrow(c^3\Pi_u, v=2)$ transition series in Figure VII-2.

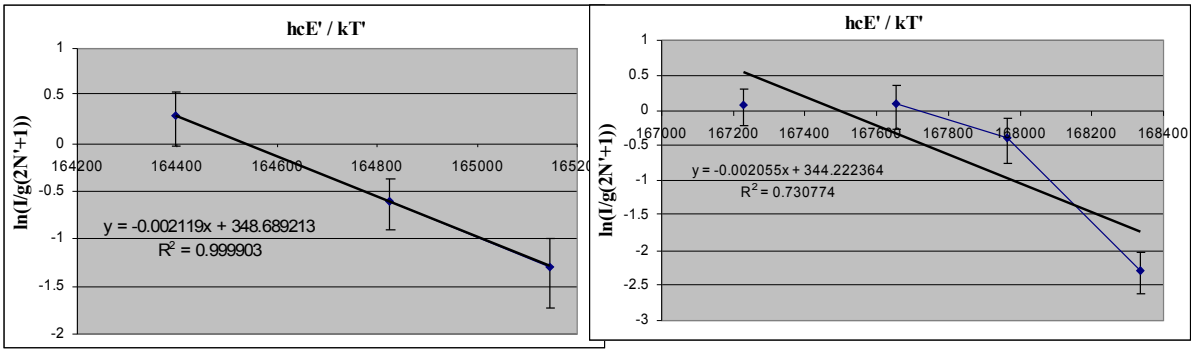

Figure VII- 2: Two useful molecular line transition series at 900 W and 0.06 T. These transition series exist between 583.8-593.9 nm on the left, and 591.6-600.6 nm on the right.

The two different transitions will yield two somewhat different temperatures, but these temperatures are reasonably averaged together to further reduce the effects of noise that can perturb the diagnosis. The results of this analysis is illustrated in Figure VII-3.

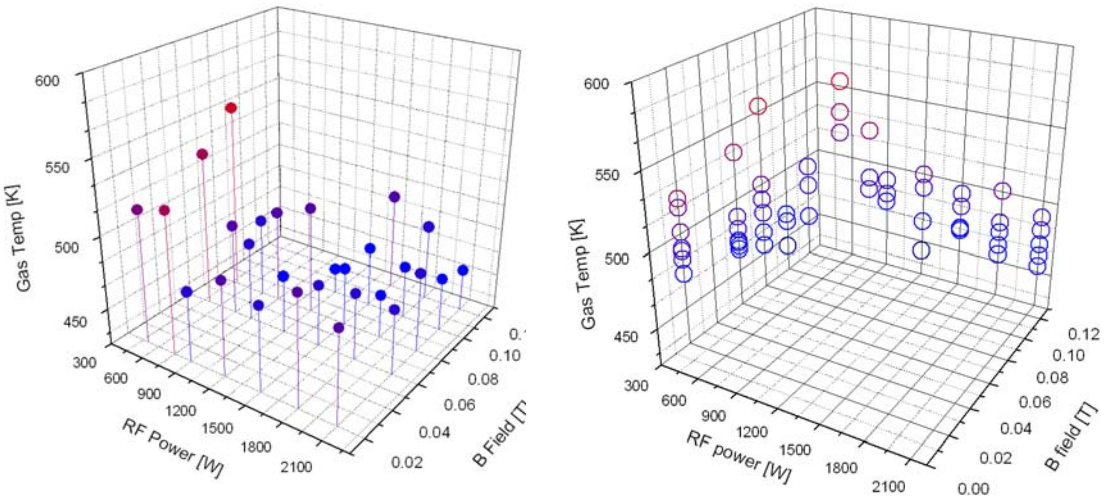

Figure VII-3: The gas temperature in the helicon source, in kelvin, for a variety of helicon source operating conditions. These values were determined using the molecular line transition diagnosis approach. On the left are points for gas temperature in the RF Power [W] and B field [T] operation space, and on the right these values are projected onto the vertical planes.

Error analysis of these measurements is carried out by assessing the error in the calculation of the slope [VII-3] from which the temperature is calculated, using Equation (VII-2).

$$\sigma_y = \sqrt{\frac{1}{N-2}\sum_{i=1}^{N}(y_i - b - m x_i)^2}$$
$$\Delta = N\sum_{i=1}^{N} x_i^2 - \left(\sum_{i=1}^{N} x_i\right)^2 \qquad \text{(VII-2)}$$
$$\sigma_b = \sigma_y \sqrt{\frac{\sum_{i=1}^{N} x_i^2}{\Delta}}$$

Where σ_y is the standard error of the fit to an individual measurement, N is the number of measurements, y_i is an individual measurement, b is the y-intercept of the linear fit, m is the slope, x_i is the independent variable, and σ_b is the uncertainty in the slope of the linear fit.

The results of this error calculation are illustrated in Figure VII-4.

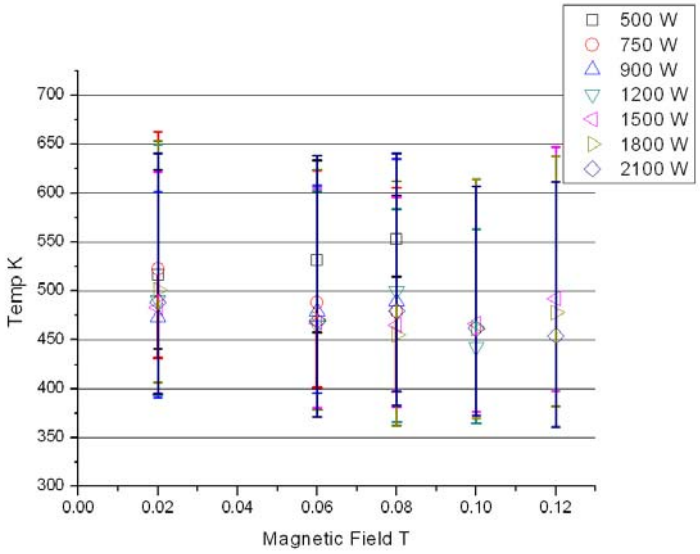

Figure VII-4: The measured gas temperatures, with calculated error bars, across the magnetic field.

Comparison of the optical results with a thermocouple measurement of the helicon source quartz tube during operation provides a rough confirmation of the optical method of gas temperature measurement. An equilibrium is reached between the heat sources and sinks producing the measured equilibrium helicon source temperature, but characterizing these relations is nontrivial. As a result, this measurement can only serve as a rough order of magnitude check and as a way of characterizing the difference in temperature between power levels. Much like the optical measurements showed of the gas, the temperature of the quartz tube did not vary significantly over the operation range, and generally were in the 400 K range, as illustrated in Figure VII-5.

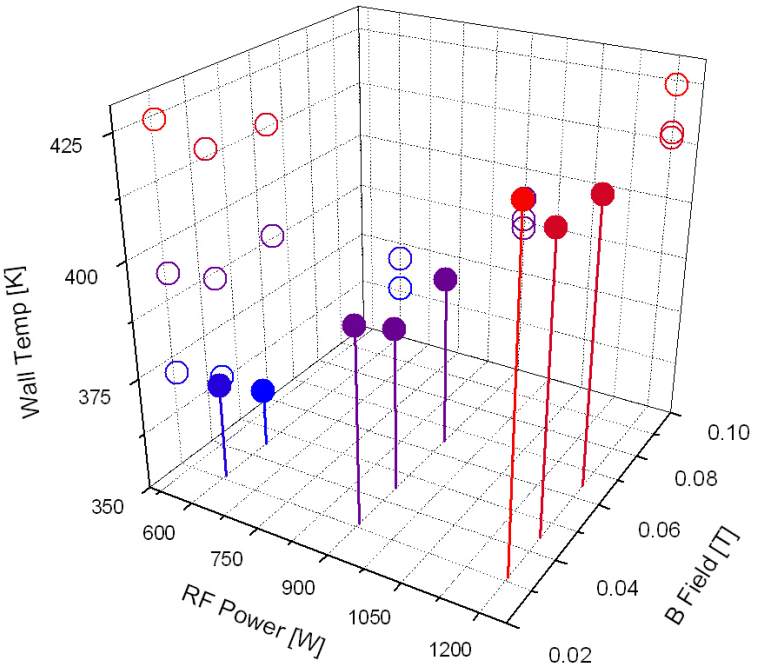

Figure VII-5: The temperature of the helicon source quartz tube as measured by a high temperature thermocouple for a variety of operating conditions. The open symbols are projections of the thermocouple data onto the vertical planes. These values were measured directly.

VII-C) Helicon Source Gas Pressure and Density Diagnosis

Using conduction theory, as outlined in Chapter III-C, pump speed for the relevant gas, and the measured down stream chamber pressure, the helicon source gas pressure has been obtained. The downstream pressure was measured by a Varian ion gauge. Results of this calculation are illustrated in Figure VII-6.

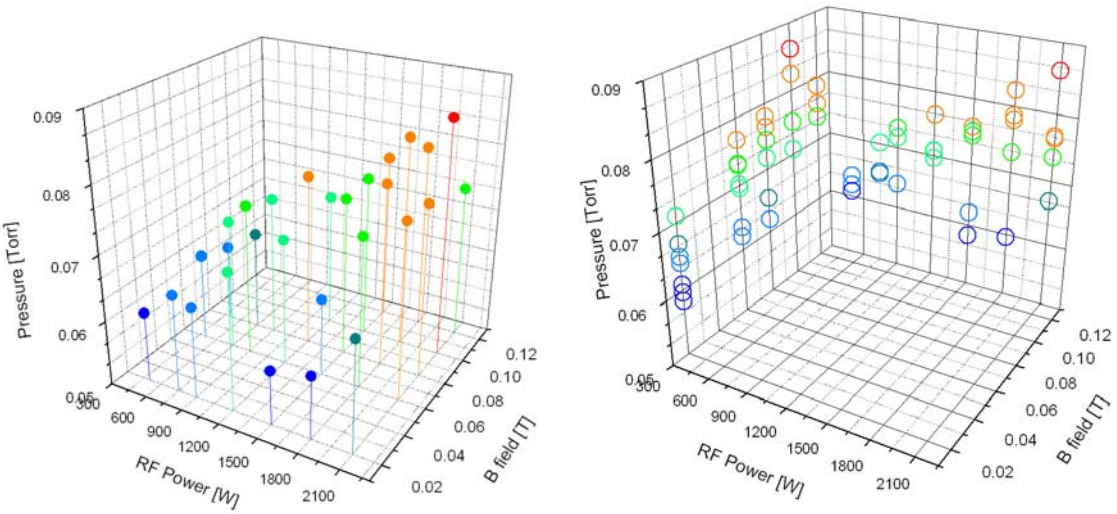

Figure VII- 6: The derived helicon source gas pressure, in torr, for a variety of helicon source operation conditions. These values were determined using conduction theory, downstream pump speed and downstream chamber pressure. On the left are points for gas pressure in the RF Power [W] and B field [T] operation space, and on the right these values are projected onto vertical planes.

Obtaining the helicon source gas pressure along with determined gas temperature allowed for the determination of the helicon source gas density, using the ideal gas law, as outlined in Chapter III-C. The results of this gas density calculations are illustrated in Figure VII-7.

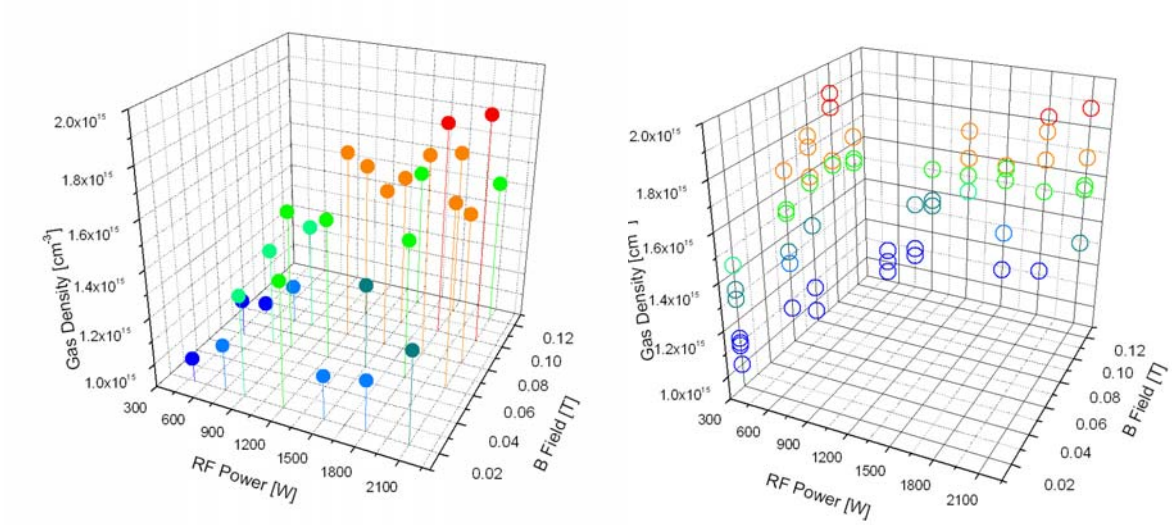

Figure VII- 7: The derived gas density in the helicon source, in cm^{-3}, for a variety of helicon source operation conditions. These values were determined using gas temperature and measured downstream pressure. On the left are points for gas density in the RF Power [W] and B field [T] operation space, and on the right these values are projected onto vertical planes.

VII-D) Atomic to Molecular Species Ratio Diagnosis

In low pressure hydrogen discharges, determining the atomic and molecular species from CR modeling is theoretically straightforward. Measuring two independent intensity ratios and determining the conditions where the modeled parameters match produces results in agreement with the data to characterize the plasma conditions. However, there are regimes where the emitted lines are not discernibly dependent on electron temperature or atomic to molecular species ratio.

The ratios studied by Lavrov [VII-1] in hydrogen discharges, $I_{H\alpha}/I_{H\beta}$ and $I_{H\alpha}/I_{Q1}$, have clear regimes of insensitivity to electron and atomic to molecular species. Unfortunately, for the electron temperature regime above 5 eV, in which the helicon source typically operates, the $I_{H\alpha}/I_{H\beta}$ ratio is insensitive to both of these parameters when the H/H_2 ratio is above 1:1, as is evidenced by Figure VII-8 [VII-1].

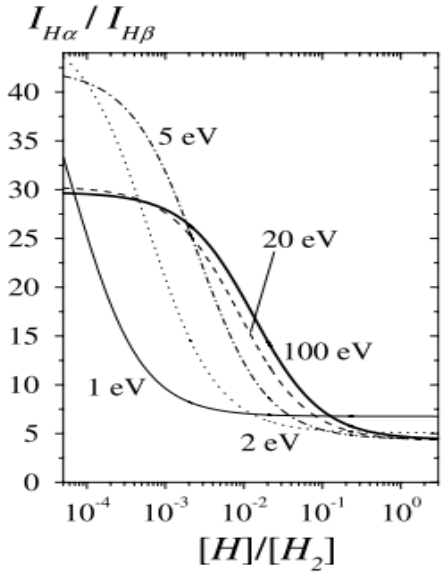

Figure VII-8: The H_α and H_β intensity ratios as dependent on the hydrogen atomic to molecular ratio, for a variety of electron temperatures, calculated by Lavrov [VII-1].

As can be seen, at high atomic to molecular ratios the emission intensity ratio is between 4 and 7 for all electron temperatures above 2 eV. In a high power and density helicon source hydrogen plasma the atomic to molecular ratio is expected to be high. However, the $I_{H\beta}/I_{Q1}$ ratio remains sensitive to both electron temperature and atomic to molecular ratio in this regime, as evidenced in Figure VII-9.

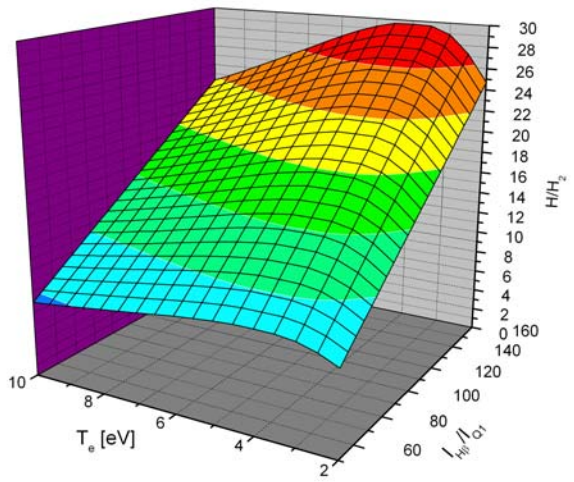

Figure VII-9: Possible N_H/N_{H2} ratio for the regime $I_{H\beta}/I_{Q1}$ ratios observed across all typically observed helicon source electron temperatures, using the values generated and presented by Lavrov [VII-1].

For this helicon source's operating regime, the electron temperature cannot be defined at this point in the diagnosis. This is unfortunate, but not ruinous to the diagnosis of the helicon source plasma density ratio. The profile of the N_H/N_{H2} ratio is relatively flat across possible electron temperatures; this allows the atomic to molecular fraction to be defined with roughly 20% uncertainty.

Previous work leads us to believe the electron temperature is roughly 5 eV, as previous diagnostics have found this temperature common at lower densities for a variety of plasma species and helicon source settings [VII-4,5]. Using the electron temperature of 5

eV, the H/H_2 ratio parameter space of the helicon source can then be mapped as illustrated in Figure VII-10.

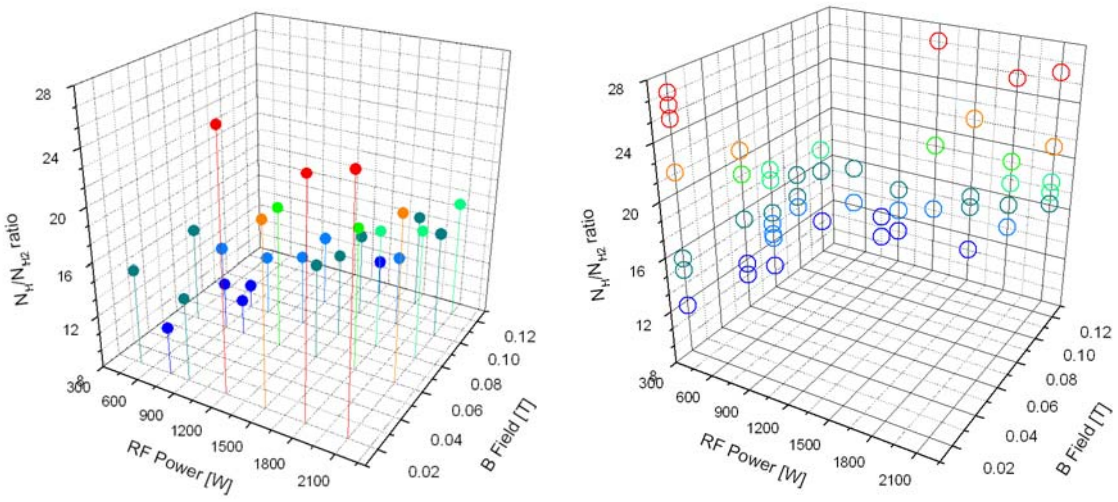

Figure VII- 10: Determined H/H2 ratio in the helicon source for a variety of operation conditions. These values were found comparing the Q1molecular line and H_β line intensity ratio at each operation point with the intensity ratios predicted by the rate coefficients calculated by Lavrov, as listed in Table IV-1. On the left are points for gas pressure in the RF Power [W] and B field [T] operation space, and on the right these values are projected onto vertical axes.

VII-E) Electron Density and Temperature Diagnosis

The electron density and temperature diagnosis is achieved utilizing Sawada's CR model [VII-6,7,8,9,10], as discussed in Chapter IV-D. This code was used to generate a matrix of transition rates, dependent on electron temperature in eV and electron density in cm^{-3}. These rates are used to generate intensity ratios, as discussed in Chapter IV-D. Some of the calculated transition rates predicted from Sawada's code are listed in the following tables. Table VII-1 lists the predicted transition rates of the atomic hydrogen $4 \rightarrow 2$ transition (Balmer Beta transition), here called $R(H_\beta)$. Table VII-2 lists the predicted

transition rates of the molecular hydrogen $4 \rightarrow 2$ transition (Balmer Beta transition), here called R($H_{2\text{-}\beta}$).

R(H_β)																
$T_e \backslash n_e$ $eV \backslash cm^{-3}$	8E+10	9E+10	1E+11	2E+11	3E+11	4E+11	5E+11	6E+11	7E+11	8E+11	9E+11	1E+12	2E+12	3E+12	4E+12	5E+12
2	1.390 E-19	1.390 E-19	1.380 E-19	1.330 E-19	1.300 E-19	1.270 E-19	1.240 E-19	1.210 E-19	1.180 E-19	1.160 E-19	1.140 E-19	1.110 E-19	9.450 E-20	8.320 E-20	7.490 E-20	6.860 E-20
3	1.130 E-18	1.130 E-18	1.120 E-18	1.080 E-18	1.050 E-18	1.020 E-18	9.910 E-19	9.660 E-19	9.430 E-19	9.210 E-19	9.000 E-19	8.810 E-19	7.350 E-19	6.390 E-19	5.710 E-19	5.190 E-19
4	3.290 E-18	3.280 E-18	3.260 E-18	3.130 E-18	3.030 E-18	2.930 E-18	2.850 E-18	2.770 E-18	2.700 E-18	2.630 E-18	2.570 E-18	2.510 E-18	2.080 E-18	1.800 E-18	1.600 E-18	1.450 E-18
5	6.310 E-18	6.280 E-18	6.250 E-18	5.990 E-18	5.780 E-18	5.600 E-18	5.430 E-18	5.280 E-18	5.140 E-18	5.010 E-18	4.880 E-18	4.770 E-18	3.920 E-18	3.380 E-18	3.000 E-18	2.720 E-18
6	9.810 E-18	9.760 E-18	9.710 E-18	9.300 E-18	8.970 E-18	8.680 E-18	8.420 E-18	8.170 E-18	7.950 E-18	7.750 E-18	7.550 E-18	7.370 E-18	6.040 E-18	5.190 E-18	4.610 E-18	4.170 E-18
7							1.160 E-17	1.120 E-17	1.090 E-17	1.060 E-17	1.040 E-17	1.010 E-17	8.270 E-18	7.110 E-18	6.300 E-18	5.700 E-18

Table VII-1: The atomic transition rates of Hydrogen's Balmer β transition, for a variety of plasma parameters, as predicted by Sawada's hydrogen CR code.

R($H_{2\text{-}\beta}$)																
$T_e \backslash n_e$ $eV \backslash cm^{-3}$	8E+10	9E+10	1E+11	2E+11	3E+11	4E+11	5E+11	6E+11	7E+11	8E+11	9E+11	1E+12	2E+12	3E+12	4E+12	5E+12
2	6.534 E-22	6.518 E-22	6.502 E-22	6.357 E-22	6.227 E-22	6.108 E-22	5.997 E-22	5.893 E-22	5.795 E-22	5.702 E-22	5.613 E-22	5.529 E-22	4.865 E-22	4.407 E-22	4.068 E-22	3.804 E-22
3	1.159 E-20	1.156 E-20	1.153 E-20	1.125 E-20	1.100 E-20	1.077 E-20	1.056 E-20	1.036 E-20	1.018 E-20	1.000 E-20	9.837 E-21	9.681 E-21	8.474 E-21	7.664 E-21	7.075 E-21	6.621 E-21
4	4.944 E-20	4.929 E-20	4.915 E-20	4.789 E-20	4.677 E-20	4.575 E-20	4.481 E-20	4.393 E-20	4.311 E-20	4.234 E-20	4.162 E-20	4.094 E-20	3.571 E-20	3.225 E-20	2.976 E-20	2.785 E-20
5	1.209 E-19	1.205 E-19	1.202 E-19	1.169 E-19	1.141 E-19	1.115 E-19	1.091 E-19	1.069 E-19	1.048 E-19	1.029 E-19	1.011 E-19	9.938 E-20	8.637 E-20	7.786 E-20	7.175 E-20	6.709 E-20
6	2.244 E-19	2.237 E-19	2.230 E-19	2.168 E-19	2.114 E-19	2.064 E-19	2.018 E-19	1.976 E-19	1.937 E-19	1.900 E-19	1.866 E-19	1.833 E-19	1.587 E-19	1.428 E-19	1.313 E-19	1.226 E-19
7							1.158 E-17	1.124 E-17	1.093 E-17	1.065 E-17	1.038 E-17	1.013 E-17	8.274 E-18	7.110 E-18	6.301 E-18	5.701 E-18

Table VII-2: The molecular transition rates of Hydrogen's Balmer β transition, for a variety of plasma parameters, as predicted by Sawada's hydrogen CR code.

Similarly,Table VII-3 lists the predicted transition rates of the atomic hydrogen $5 \rightarrow 2$ transition (Balmer gamma transition), here designated $R(H_\gamma)$. Table VII-4 lists the predicted transition rates of the molecular hydrogen $5 \rightarrow 2$ transition (Balmer gamma transition), here designated $R(H_{2\text{-}\gamma})$.

$R(H_\gamma)$																
$T_e \backslash n_e$ $eV \backslash cm^{-3}$	8E+10	9E+10	1E+11	2E+11	3E+11	4E+11	5E+11	6E+11	7E+11	8E+11	9E+11	1E+12	2E+12	3E+12	4E+12	5E+12
2	1.373 E-19	1.353 E-19	1.335 E-19	1.179 E-19	1.064 E-19	9.750 E-20	9.031 E-20	8.437 E-20	7.937 E-20	7.509 E-20	7.138 E-20	6.811 E-20	4.868 E-20	3.928 E-20	3.352 E-20	2.957 E-20
3	1.167 E-18	1.149 E-18	1.131 E-18	9.893 E-19	8.865 E-19	8.078 E-19	7.452 E-19	6.939 E-19	6.510 E-19	6.145 E-19	5.830 E-19	5.554 E-19	3.926 E-19	3.148 E-19	2.675 E-19	2.352 E-19
4	3.456 E-18	3.400 E-18	3.346 E-18	2.911 E-18	2.599 E-18	2.362 E-18	2.175 E-18	2.023 E-18	1.895 E-18	1.787 E-18	1.694 E-18	1.613 E-18	1.135 E-18	9.076 E-19	7.698 E-19	6.757 E-19
5	6.706 E-18	6.594 E-18	6.487 E-18	5.628 E-18	5.017 E-18	4.554 E-18	4.189 E-18	3.892 E-18	3.645 E-18	3.436 E-18	3.256 E-18	3.098 E-18	2.176 E-18	1.738 E-18	1.473 E-18	1.292 E-18
6	1.052 E-17	1.034 E-17	1.017 E-17	8.811 E-18	7.847 E-18	7.118 E-18	6.545 E-18	6.079 E-18	5.692 E-18	5.364 E-18	5.081 E-18	4.835 E-18	3.392 E-18	2.708 E-18	2.294 E-18	2.012 E-18
7							9.064 E-18	8.418 E-18	7.881 E-18	7.426 E-18	7.035 E-18	6.693 E-18	4.694 E-18	3.746 E-18	3.173 E-18	2.782 E-18

Table VII-3: The atomic transition rates of Hydrogen's Balmer g transition, for a variety of plasma parameters, as predicted by Sawada's hydrogen CR code.

R($H_{2\text{-}\gamma}$)																
$T_e \backslash n_e$ $eV \backslash cm^{-3}$	8E+10	9E+10	1E+11	2E+11	3E+11	4E+11	5E+11	6E+11	7E+11	8E+11	9E+11	1E+12	2E+12	3E+12	4E+12	5E+12
2	4.111 E-22	4.066 E-22	4.023 E-22	3.661 E-22	3.387 E-22	3.171 E-22	2.995 E-22	2.848 E-22	2.723 E-22	2.614 E-22	2.519 E-22	2.435 E-22	1.912 E-22	1.641 E-22	1.467 E-22	1.343 E-22
3	7.318 E-21	7.235 E-21	7.154 E-21	6.487 E-21	5.992 E-21	5.607 E-21	5.295 E-21	5.037 E-21	4.818 E-21	4.629 E-21	4.464 E-21	4.318 E-21	3.414 E-21	2.947 E-21	2.647 E-21	2.433 E-21
4	3.160 E-20	3.122 E-20	3.087 E-20	2.793 E-20	2.577 E-20	2.410 E-20	2.276 E-20	2.165 E-20	2.071 E-20	1.990 E-20	1.920 E-20	1.857 E-20	1.471 E-20	1.272 E-20	1.145 E-20	1.053 E-20
5	7.857 E-20	7.763 E-20	7.672 E-20	6.930 E-20	6.387 E-20	5.969 E-20	5.634 E-20	5.357 E-20	5.123 E-20	4.922 E-20	4.746 E-20	4.590 E-20	3.633 E-20	3.139 E-20	2.822 E-20	2.596 E-20
6	1.485 E-19	1.467 E-19	1.449 E-19	1.307 E-19	1.203 E-19	1.124 E-19	1.060 E-19	1.007 E-19	9.626 E-20	9.244 E-20	8.910 E-20	8.615 E-20	6.798 E-20	5.862 E-20	5.263 E-20	4.836 E-20
7							1.700 E-19	1.615 E-19	1.543 E-19	1.481 E-19	1.426 E-19	1.379 E-19	1.084 E-19	9.327 E-20	8.358 E-20	7.669 E-20

Table VII-4: The molecular transition rates of Hydrogen's Balmer γ transition, for a variety of plasma parameters, as predicted by Sawada's hydrogen CR code.

Finally, Table VII-5 lists the predicted transition rates of the atomic hydrogen $6 \rightarrow 2$ transition (Balmer delta transition), here designated R(H_δ). Table VII-6 lists the predicted transition rates of the molecular hydrogen $6 \rightarrow 2$ transition (Balmer delta transition), here designated R($H_{2\text{-}\delta}$).

$R(H_\delta)$																
$T_e \backslash n_e$ $eV \backslash cm^{-3}$	8E+10	9E+10	1E+11	2E+11	3E+11	4E+11	5E+11	6E+11	7E+11	8E+11	9E+11	1E+12	2E+12	3E+12	4E+12	5E+12
2	1.207 E-19	1.162 E-19	1.122 E-19	8.547 E-20	7.076 E-20	6.120 E-20	5.437 E-20	4.921 E-20	4.514 E-20	4.183 E-20	3.908 E-20	3.674 E-20	2.420 E-20	1.882 E-20	1.571 E-20	1.365 E-20
3	1.041 E-18	1.001 E-18	9.651 E-19	7.293 E-19	6.014 E-19	5.188 E-19	4.602 E-19	4.159 E-19	3.810 E-19	3.527 E-19	3.292 E-19	3.093 E-19	2.026 E-19	1.569 E-19	1.306 E-19	1.132 E-19
4	3.106 E-18	2.986 E-18	2.878 E-18	2.169 E-18	1.786 E-18	1.539 E-18	1.365 E-18	1.233 E-18	1.129 E-18	1.045 E-18	9.750 E-19	9.159 E-19	5.987 E-19	4.631 E-19	3.850 E-19	3.334 E-19
5	6.063 E-18	5.827 E-18	5.615 E-18	4.226 E-18	3.480 E-18	2.999 E-18	2.658 E-18	2.401 E-18	2.199 E-18	2.035 E-18	1.899 E-18	1.784 E-18	1.166 E-18	9.011 E-19	7.489 E-19	6.483 E-19
6	9.556 E-18	9.184 E-18	8.848 E-18	6.660 E-18	5.484 E-18	4.727 E-18	4.190 E-18	3.785 E-18	3.467 E-18	3.209 E-18	2.994 E-18	2.813 E-18	1.838 E-18	1.421 E-18	1.181 E-18	1.022 E-18
7							5.845 E-18	5.282 E-18	4.838 E-18	4.479 E-18	4.180 E-18	3.927 E-18	2.568 E-18	1.985 E-18	1.650 E-18	1.428 E-18

Table VII-5: The atomic transition rates of Hydrogen's Balmer δ transition, for a variety of plasma parameters, as predicted by Sawada's hydrogen CR code.

$R(H_{2\text{-}\delta})$																
$T_e \backslash n_e$ $eV \backslash cm^{-3}$	8E+10	9E+10	1E+11	2E+11	3E+11	4E+11	5E+11	6E+11	7E+11	8E+11	9E+11	1E+12	2E+12	3E+12	4E+12	5E+12
2	1.373 E-19	1.353 E-19	1.335 E-19	1.179 E-19	1.064 E-19	9.750 E-20	9.031 E-20	8.437 E-20	7.937 E-20	7.509 E-20	7.138 E-20	6.811 E-20	4.868 E-20	3.928 E-20	3.352 E-20	2.957 E-20
3	1.167 E-18	1.149 E-18	1.131 E-18	9.893 E-19	8.865 E-19	8.078 E-19	7.452 E-19	6.939 E-19	6.510 E-19	6.145 E-19	5.830 E-19	5.554 E-19	3.926 E-19	3.148 E-19	2.675 E-19	2.352 E-19
4	3.456 E-18	3.400 E-18	3.346 E-18	2.911 E-18	2.599 E-18	2.362 E-18	2.175 E-18	2.023 E-18	1.895 E-18	1.787 E-18	1.694 E-18	1.613 E-18	1.135 E-18	9.076 E-19	7.698 E-19	6.757 E-19
5	6.706 E-18	6.594 E-18	6.487 E-18	5.628 E-18	5.017 E-18	4.554 E-18	4.189 E-18	3.892 E-18	3.645 E-18	3.436 E-18	3.256 E-18	3.098 E-18	2.176 E-18	1.738 E-18	1.473 E-18	1.292 E-18
6	1.052 E-17	1.034 E-17	1.017 E-17	8.811 E-18	7.847 E-18	7.118 E-18	6.545 E-18	6.079 E-18	5.692 E-18	5.364 E-18	5.081 E-18	4.835 E-18	3.392 E-18	2.708 E-18	2.294 E-18	2.012 E-18
7							9.064 E-18	8.418 E-18	7.881 E-18	7.426 E-18	7.035 E-18	6.693 E-18	4.694 E-18	3.746 E-18	3.173 E-18	2.782 E-18

Table VII-6: The molecular transition rates of Hydrogen's Balmer δ transition, for a variety of plasma parameters, as predicted by Sawada's hydrogen CR code.

While, these results can be generated easily by Sawada's code, the results listed in these tables do not appear in the literature to the knowledge of the author. These values, the

atomic to molecular ratio, and the equations from Chapter IV-D can be used to check the validity of Sawada's code as it applies to a particular hydrogen plasma under study via consistent agreement between model and observation across multiple intensity ratios. Sawada's code generates these values to higher precision, which is useful for the actual diagnosis.

Using these model results, the plasma electron density and temperatures for some operation conditions were obtained. A matrix of theoretical intensity ratios for a series of densities for multiple temperatures, as dependent on the atomic to molecular hydrogen ratio, is simple to produce. The values of these ratios are then compared against the observed intensity ratios, and points of multiple agreement denotes a successful application of the model to produce a diagnosis. An example of a successful diagnosis is illustrated in Figure VII-11.

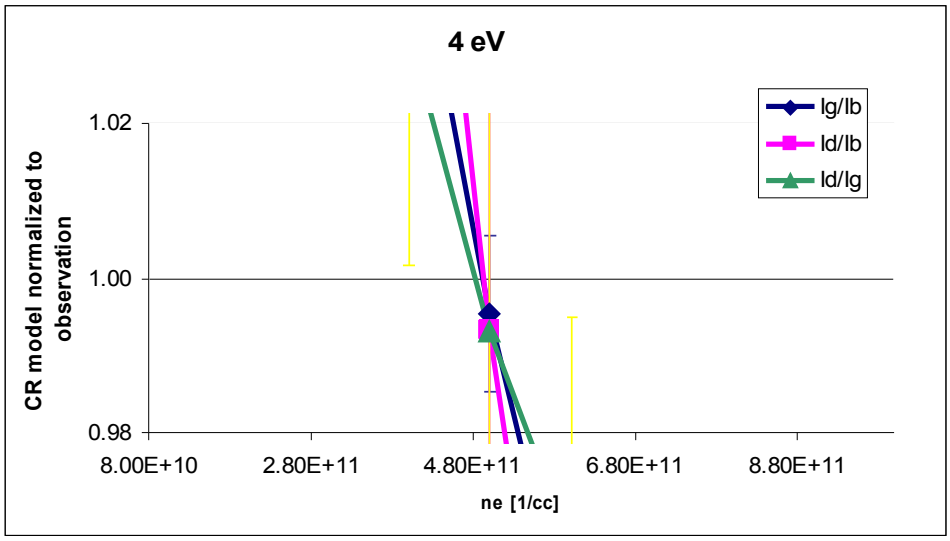

Figure VII-11: The diagnosis of the helicon source hydrogen plasma at 500 W and 0.06 T. The CR model prediction and the observed intensity ratios for this plasma agree for conditions of a 4 eV electron temperature and about $5x10^{11}$ electrons cm^{-3}. In this figure, Ig/Ib is the ratio of the intensity of the Balmer γ line and Balmer β line, divided by the predicted ratio generated by Sawada's code at each electron density (so that agreement between observation and model occurs at 1.00). Similarly, Id/Ib represents the same, but for the Balmer δ line and Balmer β line ratio; Id/Ig represents the same, but for the Balmer δ line and Balmer γ line ratio.

The results of this analysis on all points of operation yields a partial picture of the properties of the electron population in the hydrogen plasma. These results are illustrated in Figure VII- for electron density, and Figure VII-13 for electron temperature.

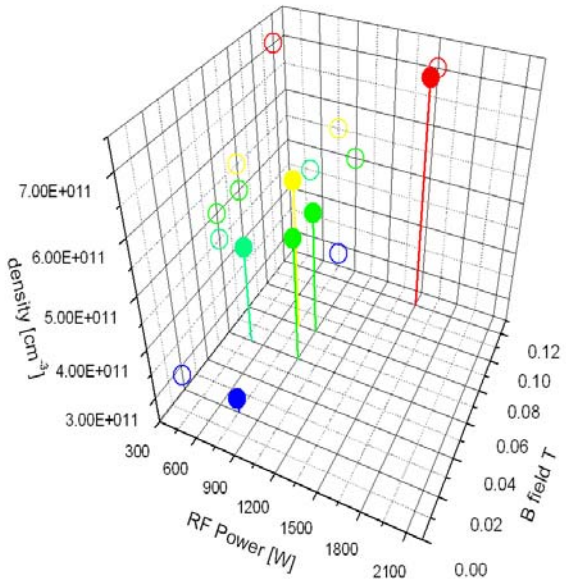

Figure VII-12: Electron density, in cm^{-3}, for a variety of helicon source operation conditions. These values were determined comparing H_β, H_γ, H_δ intensity ratios at each operation point with the intensity ratios predicted by the rate coefficients calculated by Sawada's CR code.

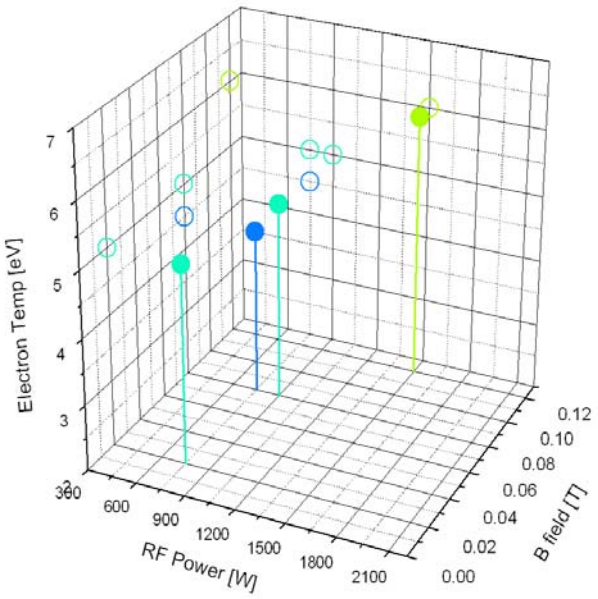

Figure VII-13: Electron temperature, in eV, for a variety of helicon source operation conditions. These values were determined comparing H_β, H_γ, H_δ intensity ratios at each operation point with the intensity ratios with the intensity ratios predicted by the rate coefficients calculated by Sawada's CR code.

References for Chapter VII

VII-1 B. P. Lavrov, A. V. Pipa, and J. Ropcke, "On determination of the degree of dissociation of hydrogen in non-equilibrium plasmas by means of emission spectroscopy: I. The collision-radiative model and numerical experiments," Plasma Sources Science & Technology 15.1 (2006): 135-46.

VII-2 SA Astashkevich, et al, "Radiative characteristics of 3p Sigma, Pi; 3d Pi-, Delta-states of H2 and determination of gas temperature of low pressure hydrogen containing plasmas," Journal of Quantitative Spectroscopy and Radiative Transfer 56.5 (1996): 725-51.

VII-3 P. R. Bevington, D. K. Robinson, and G. Bunce, "Data Reduction and Error Analysis for the Physical Sciences," American Journal of Physics 61 (1993): 766.

VII-4 RF Boivin, JL Kline, and EE Scime, "Electron temperature measurement by a helium line intensity ratio method in helicon plasmas," Physics of Plasmas 8 (2001): 5303.

VII-5 MD Carter, et al, "Comparing experiments with modeling for light ion helicon plasma sources," Physics of Plasmas 9 (2002): 5097.

VII-6 T. Fujimoto, S. Miyachi, and K. Sawada, "New density diagnostic method based on emission line intensity ratio of neutral hydrogen in an ionizing phase plasma," Nuclear Fusion 28.7 (1988): 1255-63.

VII-7 T. Fujimoto, K. Sawada, and K. Takahata, "Ratio of Balmer line intensities resulting from dissociative excitation of molecular hydrogen in an ionizing plasma," Journal of Applied Physics 66 (1989): 2315.

VII-8 K. Sawada, K. Eriguchi, and T. Fujimoto, "Hydrogen-atom spectroscopy of the ionizing plasma containing molecular hydrogen: Line intensities and ionization rate," Journal of Applied Physics 73 (1993): 8122.

VII-9 K. Sawada and T. Fujimoto, "Effective ionization and dissociation rate coefficients of molecular hydrogen in plasma," Journal of Applied Physics 78 (1995): 2913.

VII-10 Private correspondence with Dr.Sawada 10/4/2007

VIII-A) Discussion of Results – Introduction

The remote diagnosis of the helicon source hydrogen plasma has yielded encouraging results. This chapter discusses these results, beginning with the gas temperature and gas pressure, and briefly the gas density derived from these values. Next, the hydrogen atomic to molecular ratio is discussed. Finally, there is consideration of the diagnosed electron density and temperature and how these values compare to other diagnosed helicon source hydrogen plasmas.

VIII-B) Helicon Source Gas Temperature and Density Discussion

The observed molecular lines had consistent profile shape, lending confidence to the molecular line measurement. This was initially of some concern, considering the method of noise reduction in the helicon source was averaging and the line intensities were relatively weak, but at all RF power levels and magnetic field strengths the emission profiles of the molecular lines remained similar and uniformly resolvable.

Some care was taken in omitting lines from molecular transition series, as they were not resolvable from neighboring lines. Also, there were molecular lines that were consistently skewed and were omitted from the optical gas temperature analysis. These lines were identified by observing that some lines were consistently far from the linear trend of the other lines in the series.

The helicon source gas temperature is measured between 450 K and 575 K, with error

bars generally on the order 100 K. This is generally in line with the measured helicon source quartz tube temperature. For most of the readings, the temperature did not seem to be strongly dependent on RF power or magnetic field; for the majority of operation the observed gas temperature was below 500 K, notably above room temperature.

One non-intuitive observation was that the highest temperature readings were observed at the lowest power setting that achieved a breakdown, 500 W. The downstream gas pressure, measured via ion gauge, increased with RF power and magnetic field, though the gas flow into the helicon source was held constant. As the ion gauge is a highly reliable pressure measurement, and the gas flow into the helicon source was held constant, it is safe to conclude the majority of the helicon source gas actually increases with temperature. This leaves the question of why the optical gas temperature measurement showed increased gas temperature at the RF Power 500 W setting.

The helicon source matching circuit attempts to adjust the system coupling when there is more than 1% reflected power, so RF coupling to the plasma is not likely to play a dominant role in this observation. It is more likely the observation of the molecular lines was dominated by an effect that was concentrated at the higher radius regions of the plasma column. The measurements taken observed the plasma column perpendicular to the quartz tube, gathering light from the plasma without selecting the radius. This observation can be dominated by the outer cylindrical volume of the plasma, skewing the gas temperature results.

It is also worth noting that at low power and magnetic field the plasma was visually observed to have filled the entire helicon source quartz tube. At higher power and magnetic

field the plasma was more centrally confined to a narrow, dense, plasma column. This dense region was brighter than the diffuse plasma surrounding it, and would dominate the emission spectrum. This column is centered on the axis of the helicon source tube, and aligned with the helicon source outlet. For this reason, we conclude that the gas temperature of the higher power and magnetic field more accurately reflects the gas temperature of the region of interest, the dense plasma region, from which plasma is extracted for application. The gas pressure diagnosis of the helicon source produced a satisfying result, in that the gas pressure increases with applied RF power and magnetic field.

The gas density derived from the pressure and temperature diagnoses is between $1x10^{15}$ to $2x10^{15}cm^{-3}$. The change in pressure was not marked, but clearly trended to increase with power and pressure. From this it is clear that the derived gas density was dominated by the gas pressure.

VIII-C) Hydrogen Atomic to Molecular Ratio Discussion

The atomic to molecular density diagnosis showed consistent behavior across the helicon source operation, as illustrated in Figure VIII-1. The lowest diagnosed atomic to molecular density ratio was about 10 and the highest was about 27, with noticeable scatter in the operation space. There were two trends in the atomic to molecular ratio which increased with RF Power and decreased with magnetic field. This could be an effect of the high density plasma column taking up less helicon source volume at high magnetic field, or an

interplay between the electron density and temperature.

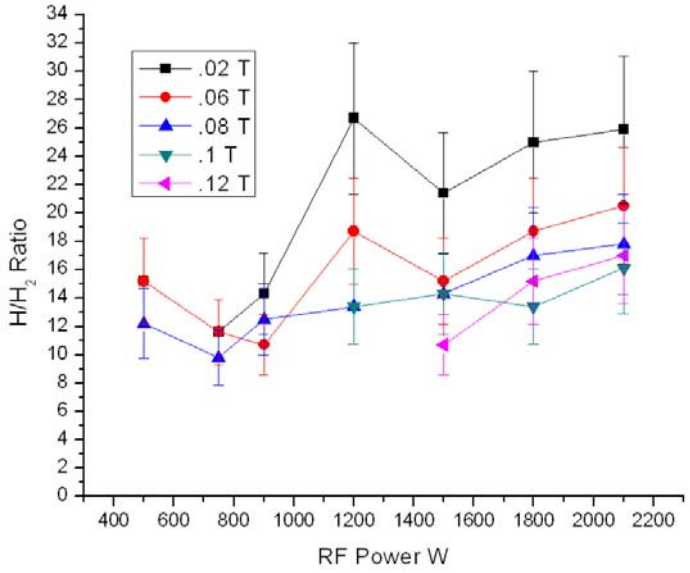

Figure VIII-1: Atomic to molecular ratio of hydrogen in the helicon source plasma for a variety of helicon source settings.

VIII-D) Electron Temperature and Density Diagnosis Discussion

The electron temperature and density diagnosis was carried out simultaneously. Due to this multiplicity of free parameters, the approach to diagnosing these characteristics was necessarily broad. This necessitated the generation of many transition rates.

The transition rates were used to produce a matrix of theoretical intensity ratios, with electron temperature and density as input parameters. These parameters were divided by the

observed intensity ratios to produce a matrix of theoretical intensity ratios normalized to the observed ratio, making searching for common agreement easier. In principle this produces three surfaces in electron temperature, electron density, and theoretical intensity ratios normalized to the observed ratio operation space, where common intersection of all three surfaces denotes the plasma condition. Analysis was eased by looking at graphs of electron density vs. normalized intensity ratio at common electron temperatures. Only cases with agreement of all three ratios were considered to produce a satisfactory analysis.

Unfortunately, these diagnoses were not as broadly successful as the other diagnoses. At many helicon source settings the observations of the helicon source plasma produced emission ratios that did not agree with the prediction derived from the transition rates produced by Sawada's hydrogen CR model. There are a variety of reasons why this could be the case, but presumably a physical interaction occurs in the helicon source plasma that is not accounted for in Sawada's CR model.

The calculated emission ratios and observed ratios in many cases agreed within an order of magnitude of electron density but it was not felt that this was sufficient for a confident diagnosis. Further, an agreement within the error bars of the intensity ratio manifested in some instances, but this was also rejected as confident result. However, in the instances where calculated intensity ratios and observed intensity ratios agreed uniquely and with high precision, it is felt the model adequately fits the observed plasma. Because multiple intensity ratios uniquely agreed with the results of the CR model, and this occurred in multiple instances it is felt that these values reflect an accurate result.

The fact that the diagnosed electron temperatures and densities conform to the results

found in other studies lends credibility to the results found here. As seen in Figures VIII-2 and VIII-3, other hydrogen helicon sources have produced plasma densities of the same order as densities measured in the helicon source under study[VIII-1,2,3].

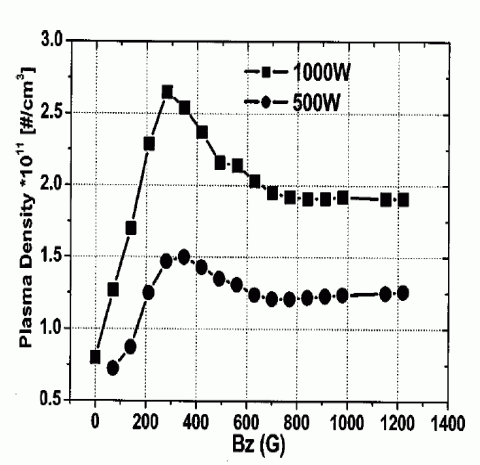

Figure VIII-2: Measured helicon source hydrogen plasma, produced by Jung et al. [VIII-1].

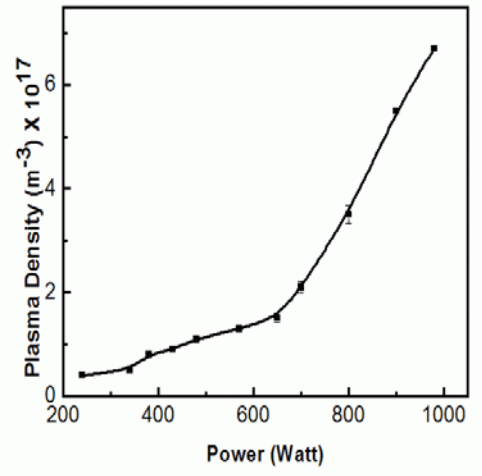

Figure VIII-3: Measured helicon source hydrogen plasma, produced by Ghosh et al. These measurements were produced at 0.041 T [VIII-2].

As an ion source, the helicon source under study has provided a maximum ion current

in hydrogen of 26 mA [VIII-4], and a maximum ion current in deuterium of 30 mA [VIII-5]. An important objective going into this diagnostic campaign was determining the charged particle density to assess the current this helicon source should be able to provide when ion extraction is optimized. The maximum ion current extracted through a hole is limited to the Bohm current[VIII-4], as expressed in equation (VIII-1):

$$I = CnqA\left(\frac{kT}{m}\right)^{\frac{1}{2}} \qquad \text{(VIII-1)}$$

where n is density, q is ion charge, A is aperture area, k is Boltzmann's constant, T is the plasma temperature, and m is the ion mass. C is a unitless constant that is dependent on plasma collisionality, that varies from 0.61 to 0.3. The helicon source's aperture area remained fixed at 0.6 cm^2.

Using the electron temperature and density we can infer the nominal ion population. For example, using the plasma parameters (observed at 900 W and 0.08 T), a 5 eV plasma temperature and ion density $5x10^{11}$ cm^{-3}, the maximum deuterium current is then between 45 and 28 mA. Using the plasma parameters (observed at 1500 W, 0.12 T), a 7 eV plasma temperature and electron density of $7x10^{11}$ cm^{-3}, the maximum predicted deuterium current is then between 75 and 38 mA. As discussed in Chapter VI-D, the maximum measured current extracted from the helicon source in deuterium is 30 mA, obtained for the helicon source settings at 1800 W and 0.11 T. This extracted current is observed to be highly dependent on the magnetic alignment with the helicon source. From this, we predict that the helicon source ion extraction has potential for improvement, and ion extraction optics in the next generation of the helicon source can be tailored to the observed plasma regime.

References for Chapter IIX

IIX-1 HD Jung, et al, "Development of a compact helicon ion source for neutron generators," Review of scientific instruments 75.5 (2004): 1878-80.

IIX-2 SN Ghosh, et al, "Study of High-Density Helicon-Plasma Generation and Measurement of the Plasma Parameters by Using a Frequency-Compensated Langmuir Probe," Journal of the Korean Physical Society 48.5 (2006): 908-13.

IIX-3 MD Carter, et al, "Comparing experiments with modeling for light ion helicon plasma sources," Physics of Plasmas 9 (2002): 5097.

IIX-4 GR Piefer, Performance of a Low-Pressure, Helicon Driven IEC 3He Fusion Device, UW Madison, PhD dissertation. December, 2006).

IIX-5 S Zenobia,University of Wisconsin, unpublished data from Helios Run 303, (9/13/2007)

IX-A) Conclusions

A campaign of plasma diagnosis for the University of Wisconsin Inertial Electrostaic Confinement (IEC) Advanced Fuels Project for the HELIOS helicon source ion source has been carried out. The results of this campaign show that the helicon source under study produces a hydrogen plasma density of the same order as similar helicon sources. This campaign was carried out using remote diagnostics, as the high density and temperature plasma environment is detrimental to the physical probes. The primary diagnostic in this campaign was a simple spectrometer, which was applied in conjunction with molecular and plasma physics models to interpret the recorded emission spectrum.

The results of this campaign recorded a variety of results:

- Helicon source gas temperatures were measured to be between 450 and 575 K using hydrogen molecular line analysis.
- Gas pressures were measured to be between 60 and 90 mtorr, and gas density in the helicon source between $1x10^{15}$ to $2x10^{15}$ cm^{-3}.
- The experimentally measured hydrogen atomic to molecular ratio in the helicon source varied between 10 and 27, depending on RF power and magnetic field.
- The helicon source plasma electron density was measured to be between 3 and 7 $x10^{11}$ cm^{-3}
- The electron temperature was measured to be between 5 and 6 eV.

These results lead us to conclude that there exists ample opportunity to optimize the ion current extracted from the helicon source plasma for application as an IEC ion source.

X-A) Possible Future Work

While the diagnosis of the helicon source has made significant gains, to the point of informing decisions on upgrades to the helicon source system, it is not yet complete. The challenges of helicon source diagnosis are numerous, but there are still avenues of diagnosis open that could be valuable to confirm the values presented here and augment the helicon source diagnosis. There are a variety of diagnostic methods that could possibly be explored, but a few stand out as feasible in the short term:

- Emission spectroscopy utilizing Abel inversion: The observation of the plasma, as outlined in Chapter VI, observed the entire diameter of the helicon source tube, yielding a view factor averaged observation, implicitly assuming an isotropic helicon source plasma. Helicon sources obviously have a radial dependence, though for most regimes the plasma emission is dominated by a dense plasma core. However, the radial profile of the measurements performed in this thesis is in principle achievable using an Abel inversion on a series of plasma column sections.
- Microwave interferometry: A line averaged electron density can be achieved using microwave interferometry. This has proved to be a robust diagnostic method in a variety of plasmas, including helicon sources. This would in fact improve the emission spectroscopy CR diagnostic, as it would reduce the degrees of freedom in the CR model, leaving electron temperature as the only parameter to be resolved.
- Carbon double probe: Carbon double probes have successfully performed in a regime comparable to the plasma parameters generated by the helicon in hydrogen; also, if properly

constructed, the probe self compensates for the RF environment. A diagnostic campaign using such a system could be carried out to determine the utility of such a probe and to compare with the results of the spectroscopic plasma diagnosis.

Appendix

Appendix A- Spectral Line Broadening Diagnosis

Extensive research has been done on line broadening analysis of plasma. This method analyses the line width of a strong spectral line, accounting for mechanisms that produce line broadening to determine a plasma density or temperature. A variety of elements of the system must be characterized carefully before the line broadening diagnosis can yield accurate results. The unperturbed radiator produces a Lorentzian distribution profile (due to the uncertainty principle), whose width must be known, to determine the total broadening. This method also requires a well characterized spectrometer, as knowing how the measuring device response broadens a line and the system's uncertainty is important. The two dominant physical broadening effects are Doppler broadening and pressure broadening.

The Doppler broadening results from thermal motion shifting the observed radiation wavelength, with respect to the radiator. Assuming the temperature distribution is Gaussian, for most plasma regimes the Doppler broadening will result in a Gaussian distribution:

$$L_d(\omega)=\frac{e^{\left(\frac{-\Delta\omega}{\omega_D}\right)^2}}{\sqrt{\pi}\,\omega_D} \tag{A-1}$$

where, $\Delta\omega$ is the frequency detuning from the rest frame transition frequency ω_o (the line width in frequency space), and ω_D is the Doppler broadening parameter is given by:

$$\omega_D=\left(\frac{2\mathrm{kT}}{Mc^2}\right)^{1/2}\omega_o \tag{A-2}$$

where T is the radiator temperature, and M is the radiator mass.

Pressure broadening in a plasma is most simply expressed as a result of electric fields from nearby electrons and ions interacting with radiating particles, causing Stark broadening. However, there are a variety of other mechanisms that can alter the pressure broadening effect in a plasma, including (but not limited to) collective fields associated with plasma waves, Van der Waals forces, and dipole-dipole interactions. As this term encompasses a great deal of physical interactions, it cannot be expressed as a general statement. The expression of the simplest case results in a Lorentz profile,

$$L(\omega)=\frac{w/\pi}{w^2+(\Delta\omega-d)^2} \tag{A-3}$$

where w is the half width-half maximum, and d is the shift.

The Doppler broadening's Gaussian profile and pressure broadening's Lorentz profile combine to produce a final observed spectra, described by a convolution of the Gaussian and Lorentz profiles:

$$L_c(\omega)=\int_{+\infty}^{-\infty} L_D(\Delta\omega')\,L(\Delta\omega-\Delta\omega')\,d\Delta\omega' \tag{A-4}$$

to produce a Voigt profile [A-1]. The relevant profiles are illustrated in Figure (A-1)

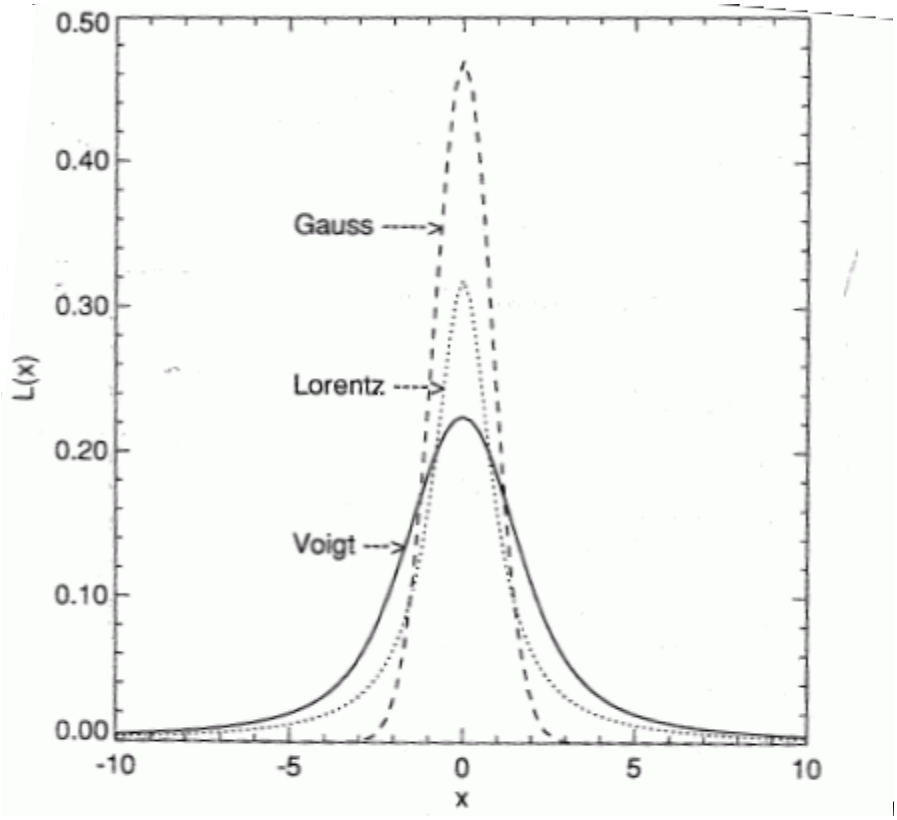

Figure A-1: Normalized Gauss (Doppler) and Lorentz (impact) profiles of equal FWHM (2 in x-units). Also shown, the resultant convolution of the two, the Voight profile [A-1].

Considering the extensive amount of foreknowledge of the plasma required before accurate diagnosis of a plasma via line broadening analysis can achieved, and the sophistication of measurement required (and associated cost), it seems that line broadening analysis would not be an appropriate plasma diagnostic method for a modest plasma laboratory study. The level foreknowledge to diagnose the plasma to a high degree of accuracy using line broadening diagnosis is impossible to obtain to a relevant level of accuracy in a high density and high temperature plasma where diagnosis by probe is limited. Further, in a modest laboratory, unless the focus of the laboratory is plasma diagnostics,

obtaining the highly accurate, low noise spectrometer is challenging.

Previous diagnostic work has been shown in various applications to yield ranges of plasma temperature and density within 1 to 4 orders of magnitude. This can be useful, particularly in astrophysics, where all measurements are necessarily remote, and the validation of theoretical work and experience is limited. However, the utility of that level of accuracy is low in a laboratory plasma, where plasma theory and previous experience already confidently ranges the plasma temperature and density with higher accuracy than the line broadening diagnostic alone can.

References for Appendix A

A-1 Hans R. Griem, Spectral line broadening by plasmas (New York: Academic Press, 1974) 408.